

Article

## Discovery of Monoiodo Aza-BODIPY Near-Infrared Photosensitizer: in vitro and in vivo Evaluation for Photodynamic Therapy

zhiliang yu, Junliang Zhou, Xin Ji, Guangyu Lin, Shuang Xu, Xiaochun Dong, and Weili Zhao

*J. Med. Chem.*, **Just Accepted Manuscript** • DOI: 10.1021/acs.jmedchem.0c00882 • Publication Date (Web): 11 Aug 2020

Downloaded from [pubs.acs.org](https://pubs.acs.org) on August 13, 2020

### Just Accepted

“Just Accepted” manuscripts have been peer-reviewed and accepted for publication. They are posted online prior to technical editing, formatting for publication and author proofing. The American Chemical Society provides “Just Accepted” as a service to the research community to expedite the dissemination of scientific material as soon as possible after acceptance. “Just Accepted” manuscripts appear in full in PDF format accompanied by an HTML abstract. “Just Accepted” manuscripts have been fully peer reviewed, but should not be considered the official version of record. They are citable by the Digital Object Identifier (DOI®). “Just Accepted” is an optional service offered to authors. Therefore, the “Just Accepted” Web site may not include all articles that will be published in the journal. After a manuscript is technically edited and formatted, it will be removed from the “Just Accepted” Web site and published as an ASAP article. Note that technical editing may introduce minor changes to the manuscript text and/or graphics which could affect content, and all legal disclaimers and ethical guidelines that apply to the journal pertain. ACS cannot be held responsible for errors or consequences arising from the use of information contained in these “Just Accepted” manuscripts.

1  
2  
3  
4  
5  
6  
7  
8  
9  
10  
11  
12  
13  
14  
15  
16  
17  
18  
19  
20  
21  
22  
23  
24  
25  
26  
27  
28  
29  
30  
31  
32  
33  
34  
35  
36  
37  
38  
39  
40  
41  
42  
43  
44  
45

# Discovery of Monoiodo Aza-BODIPY Near-Infrared Photosensitizer: *in vitro* and *in vivo* Evaluation for Photodynamic Therapy

Zhiliang Yu<sup>#, ac</sup>, Junliang Zhou<sup>#, a</sup>, Xin Ji<sup>a</sup>, Guangyu Lin<sup>a</sup>, Shuang Xu<sup>a</sup>, Xiaochun

Dong<sup>\*a</sup>, and Weili Zhao<sup>\*ab</sup>

<sup>a</sup>School of Pharmacy, Fudan University, Shanghai, 201203, P. R. China.

<sup>b</sup>Key Laboratory for Special Functional Materials of the Ministry of Education, Henan

University, Kaifeng, 475004, P. R. China.

<sup>c</sup>Shanghai Skin Disease Hospital, Shanghai, 200443, P. R. China.

46  
47  
48  
49  
50  
51  
52  
53  
54  
55  
56  
57  
58  
59  
60

**ABSTRACT:** Photodynamic therapy as a rising platform of cancer treatment method is receiving increased attention. Through systematic evaluation of halogen substitution on aza-BODIPY, we have found that monoiodo-derived aza-BODIPYs provided greater

1  
2  
3 efficacy than other halogenated aza-BODIPY PSs. **4** and **15** as monoiodinated aza-  
4  
5  
6 BODIPY dyes containing *p*-methoxyphenyl moiety were identified to be potent NIR aza-  
7  
8  
9 BODIPY type PSs with IC<sub>50</sub> values against HeLa cells at a light dose of 54 J/cm<sup>2</sup> as low  
10  
11  
12 as 76 nM, 81 nM respectively. **4** possessed superior photo-toxicity, low dark-toxicity and  
13  
14  
15 good thermal/photo stability and distributed majorly in mitochondria in cells. Apoptosis  
16  
17  
18 was verified to be the main cell death pathway and *in vitro* ROS generation was  
19  
20  
21 demonstrated. *In vivo* whole-body fluorescence imaging and *ex vivo* organ distribution  
22  
23  
24 studies suggested that **4** afforded excellent PDT effect with low drug dose under single  
25  
26  
27 time light irradiation and revealed advantages over known PSs of **ADPM06** and **Ce6**.  
28  
29  
30  
31  
32  
33  
34  
35

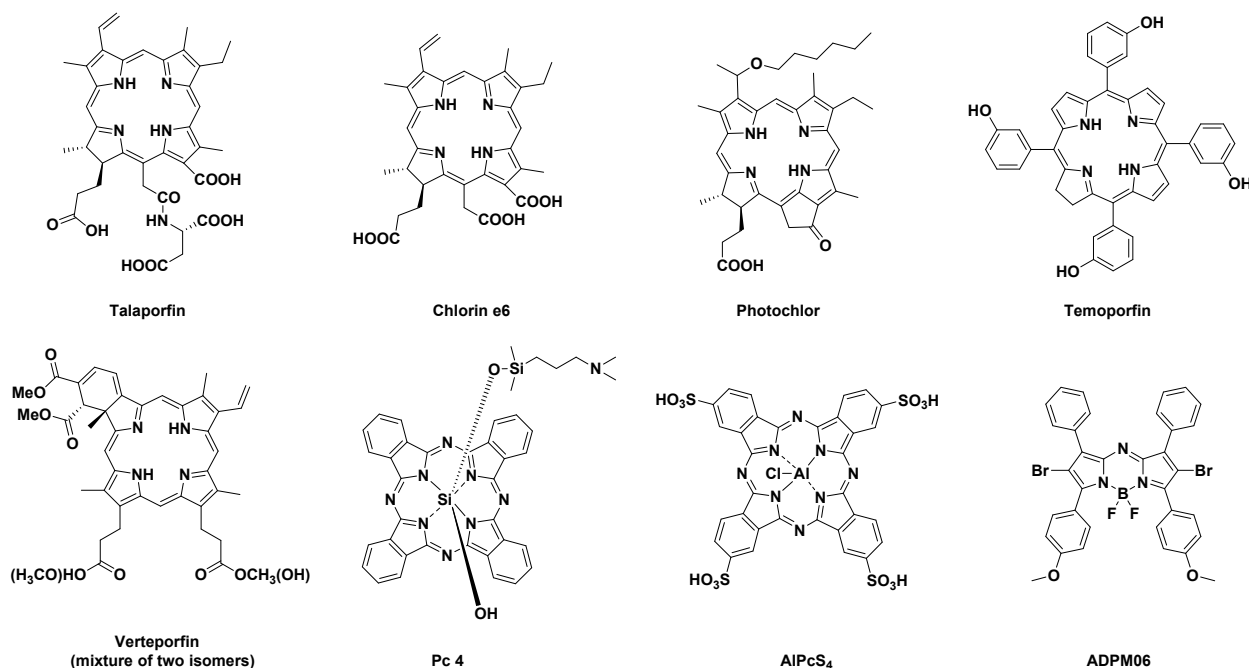
## 36 1. INTRODUCTION

37  
38  
39 Photodynamic therapy (PDT) is a rising platform of noninvasive and clinically approved  
40  
41  
42 protocol for the treatment of multiple types of cancers.<sup>1-3</sup> Three pivotal components are  
43  
44  
45 usually involved in PDT: photosensitizer (PS), light, and oxygen. The light-activated PS  
46  
47  
48 transfers its excited-state energy to either molecular oxygen (in triplet ground state) to  
49  
50  
51 form <sup>1</sup>O<sub>2</sub> (type II reaction), or to react with a biological substrate to form superoxide anion  
52  
53  
54  
55  
56  
57  
58  
59  
60

1  
2  
3 radical, hydroxyl radical, or hydrogen peroxide (type I reaction). The combined cytotoxic  
4  
5  
6  
7 reactive oxygen species (ROS) result in damage of tumor cells, tumor-associated  
8  
9  
10 vasculature infarction, and activation of immune response system.<sup>4-6</sup> Due to different  
11  
12  
13 microenvironment of tumor tissue from normal tissue, the PS administered intravenously,  
14  
15  
16  
17 intraperitoneally or locally, may be selectively retained in the tumor tissue after being  
18  
19  
20  
21 distributed for a period of time in the body.<sup>7-9</sup>  
22  
23

24 Since the clinical approval of Porfimer sodium (Photofrin), a complex mixture of  
25  
26  
27 hematoporphyrin derivatives, as PDT agent for the treatment of early and advanced  
28  
29  
30  
31 cancers,<sup>10</sup> many efforts have been focused on discovery of new photosensitizers to  
32  
33  
34  
35 overcome some deficiencies in Photofrin such as low molar absorption coefficient, poor  
36  
37  
38 bioavailability, and long-lasting cutaneous photosensitivity.<sup>11</sup> Various cyclic tetrapyrrole  
39  
40  
41 type PSs such as porphyrin, chlorin, bacterial chlorophyll, as well as phthalocyanine were  
42  
43  
44  
45 developed. Some of them have been widely used as the second-generation of PSs in  
46  
47  
48  
49 clinical treatments of cancers with improved efficacy and reduced side-effect (Fig. 1).<sup>12-14</sup>  
50  
51  
52 However, talaporfin and chlorin e6 (**Ce6**) suffered from poor photostability. Temoporfin,  
53  
54  
55  
56 photochlor and verteporfin are fairly hydrophobic with the defect of serious self-  
57  
58  
59  
60

1  
2  
3 aggregation upon administration.<sup>15,16</sup> In addition, these tetrapyrrole-based  
4  
5  
6  
7 photosensitizers, as well as phthalocyanines (**Pc 4** and **AIPcS<sub>4</sub>**), are difficult to synthesize  
8  
9  
10 and purify, therefore restricting the fine-tuning of their photophysical and chemical  
11  
12  
13 properties. Consequently, there is interest to develop non-porphyrin photosensitizers with  
14  
15  
16 ease of preparation. The focus on non-porphyrin PSs had been primarily examined on  
17  
18  
19 cationic structures such as methylene blue, Nile blue, Nile red analogues, and the  
20  
21  
22 chalcogenopyrylium class of photosensitizers. These classes of compounds, however,  
23  
24  
25  
26  
27 suffer from major drawbacks of inherent dark cytotoxicity and short absorption maxima.  
28  
29  
30  
31 In recent years, 4,4-difluoro-4-bora-3a,4a-diaza-s-indacenes (BODIPYs) have emerged  
32  
33  
34  
35 as a new class of PDT agent with many favorable characteristics.<sup>17-25</sup>  
36  
37  
38  
39  
40  
41  
42  
43  
44  
45  
46  
47  
48  
49  
50  
51  
52  
53  
54  
55  
56  
57  
58  
59  
60



26 **Figure 1.** Representative photosensitizers.

27  
28  
29  
30 BODIPYs possess many advantages of ideal photosensitizer characteristics such as  
31  
32 excellent photostability, high molar extinction coefficient, high photo-dark toxicity ratio,  
33  
34 and easy structural variation.<sup>20,22,26,27</sup> Since the early discovery of Nagano and coworkers  
35  
36 through introduction of 2,6-diiodo onto 1,3,5,7-tertramethyl BODIPY to facilitate  
37  
38 intersystem crossing to afford a potent photosensitizer with higher efficiency of singlet  
39  
40 oxygen production, as well as favorable photostability,<sup>28</sup> various BODIPY analogues  
41  
42 carrying two or more heavy atoms have been reported and demonstrated useful  
43  
44 performances on *in vitro* and *in vivo* anti-tumor studies.<sup>29-34</sup> Some of the non-halogenated  
45  
46  
47  
48  
49  
50  
51  
52  
53  
54  
55  
56  
57  
58  
59  
60

1  
2  
3  
4 BODIPYs behaved as PDT agents, unfortunately, their efficacies were fairly weak in polar  
5  
6  
7 environment.<sup>35</sup> Despite extraordinary efforts on modifications on BODIPY type PSs and  
8  
9  
10 nano-photosensitizers, they are not featured in clinical photodynamic therapy.<sup>17,18,36</sup> More  
11  
12  
13 recently, aza-BODIPYs, having the BODIPY *meso*-carbon replaced by nitrogen, attracted  
14  
15  
16 much attention due to large absorption coefficient and red-shifted absorption to fit  
17  
18  
19 therapeutic window (650–900 nm) which is clinically favored with improved tissue  
20  
21  
22 penetration of light.<sup>22</sup> One landmark for aza-BODIPY PS was disclosed by O’Shea and  
23  
24  
25 coworkers by attaching 2,6-dibromo onto 3,5-di(*p*-methoxyphenyl)-1,7-diphenyl aza-  
26  
27  
28 BODIPY as efficient NIR PS (ADPM06) as shown in Fig.1.<sup>37-38</sup> It exhibited potent  
29  
30  
31 efficacies towards a panel of cancer cell lines, as well as effective eradication of tumor  
32  
33  
34 with comparable to “cure-rates” in mice xenograft models.<sup>37-40</sup> Various examples of aza-  
35  
36  
37 BODIPY dyes carrying two or more halogen atoms were evaluated as PSs and anti-tumor  
38  
39  
40 or anti-microbial studies were examined.<sup>41-50</sup> However, incorporation of halogen to  
41  
42  
43 facilitate intersystem crossing to produce singlet oxygen may lead to increased dark  
44  
45  
46 toxicity. So far, the bottleneck to limit these aza-BODIPYs moving into clinical stage as  
47  
48  
49 non-porphyrin PSs for cancer treatment is still unclear. Up to now, there is no systemic  
50  
51  
52  
53  
54  
55  
56  
57  
58  
59  
60

1  
2  
3 investigation of the halogen effect and substitution variation on aza-BODIPY as PS for  
4  
5  
6  
7 anti-tumor study from medicinal chemistry point of view.  
8  
9

10 In this paper, a series of bromo and iodo aza-BODIPYs were synthesized based on  
11  
12  
13 3,5-di(*p*-methoxyphenyl)-1,7-diphenyl aza-BODIPY scaffold and their physical-chemical  
14  
15  
16  
17 properties were carefully evaluated. We extended our discovery in more broad range and  
18  
19  
20  
21 came to the conclusion that monoiodo derivatives of aza-BODIPY possessed various  
22  
23  
24  
25 advantages of ideal PS with excellent photostability, chemical stability and photo  
26  
27  
28 cytotoxicity. The superior antitumor efficacy was demonstrated both *in vitro* and *in vivo*.  
29  
30

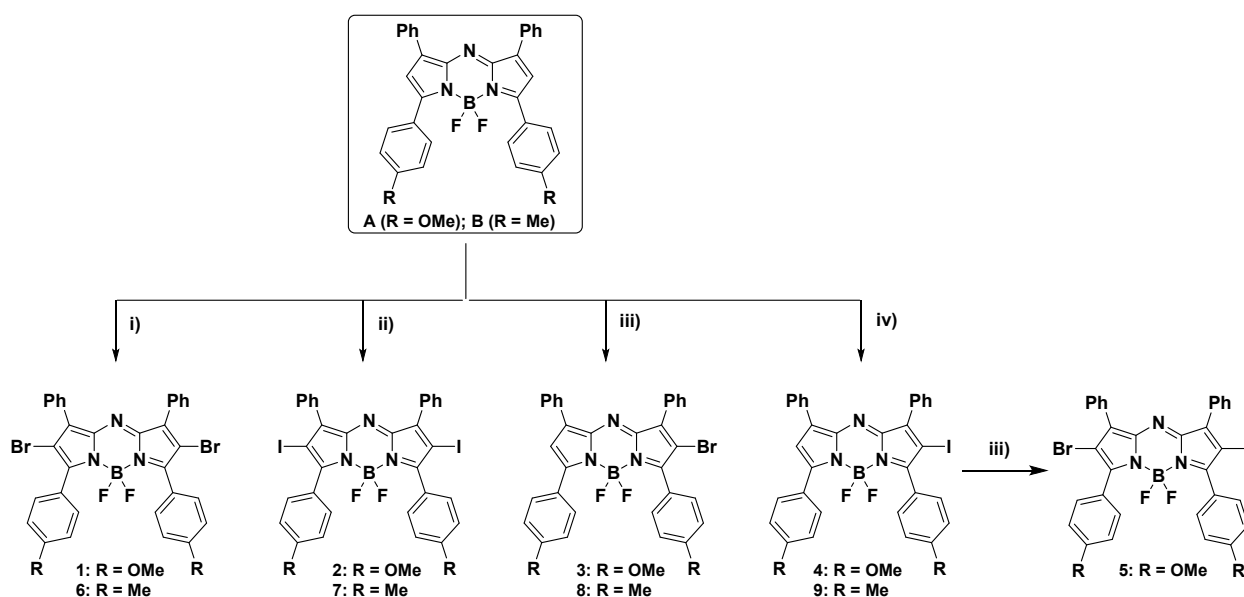
## 31 2. RESULTS AND DISCUSSION

### 32 2.1. Design and Synthesis.

33  
34  
35 Various symmetric and non-symmetric aza-BODIPY fluorescent dyes were easily  
36  
37  
38 achieved using our previous optimized methods.<sup>51-52</sup> The general known strategy to  
39  
40  
41  
42 transform aza-BODIPY dyes into PSs was to introduce heavy atoms (*e.g.* Br, I) onto both  
43  
44  
45  
46 2- and 6- positions of aza-BODIPYs.<sup>37-50</sup> The focus of our design was the comparison of  
47  
48  
49  
50  
51  
52 halogen effect by installation of mono-, di-, or mixed heavy atom(s) onto aza-BODIPY  
53  
54  
55  
56 core. Therefore, we initially selected the most advanced aza-BODIPY PS of **ADPM06** as  
57  
58  
59  
60

1  
2  
3  
4 leading compound. Various selective halogenation methods including monohalogenation,  
5  
6  
7 dihalogenation, mixed halogenation were successfully explored using 3,5-di(*p*-  
8  
9  
10 methoxyphenyl)-1,7-diphenyl aza-BODIPY (compound **A**) as the key scaffold (Scheme  
11  
12  
13  
14 1). Both dibromo PS (**1**, namely **ADPM06** by O'Shea et al.<sup>37</sup>) and diiodo PS (**2**) were  
15  
16 prepared in excellent yields (91.3%, 90.4% respectively). Monobromo PS (**3**) and  
17  
18 moniodo PS (**4**) were also obtained nicely (93.5%, 89.2% respectively). Moreover, 2-  
19  
20 bromo-6-iodo aza-BODIPY (**5**) as mixed halogenated PS was also synthesized in high  
21  
22  
23  
24  
25  
26  
27  
28  
29  
30  
31  
32  
33  
34  
35  
36  
37  
38  
39  
40  
41  
42  
43  
44  
45  
46  
47  
48  
49  
50  
51  
52  
53  
54  
55  
56  
57  
58  
59  
60

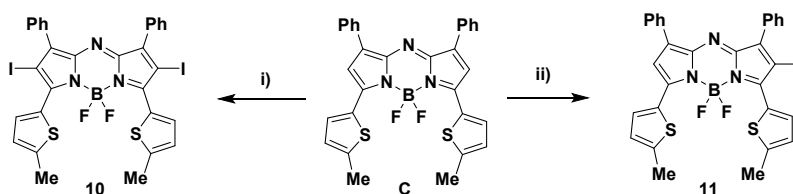
**Scheme 1.** Selective halogenation of aza-BODIPY dyes.



1  
2  
3 Reagents and conditions: i) NBS (2.2 equiv), AcOH, DCM, r.t., 30 min; ii) NIS (2.2 equiv),  
4  
5 AcOH, DCM, r.t., 30 min; iii) NBS (1.0 equiv), AcOH, DCM, r.t., 30 min; iv) NIS (1.0 equiv),  
6  
7 AcOH, DCM, r.t., 30 min.  
8  
9

10  
11  
12 We further examined the halogen effect on other NIR aza-BODIPY PSs characterized  
13  
14  
15 with electron-donation groups in broader range using 3,5-di(*p*-tolyl)-1,7-diphenyl aza-  
16  
17 BODIPY (compound **B**) as key scaffold and the halogenated PSs were similarly prepared  
18  
19  
20 BODIPY (compound **B**) as key scaffold and the halogenated PSs were similarly prepared  
21  
22  
23 as shown in Scheme 1. The generality of halogen effect was also investigated based on  
24  
25  
26 3,5-di(5'-methylthiophenyl-2-yl)-1,7-diphenyl aza-BODIPY (compound **C**) and the  
27  
28  
29 halogenated derivatives were prepared as shown in Scheme 2. All PSs were obtained in  
30  
31  
32 excellent yields.  
33  
34  
35

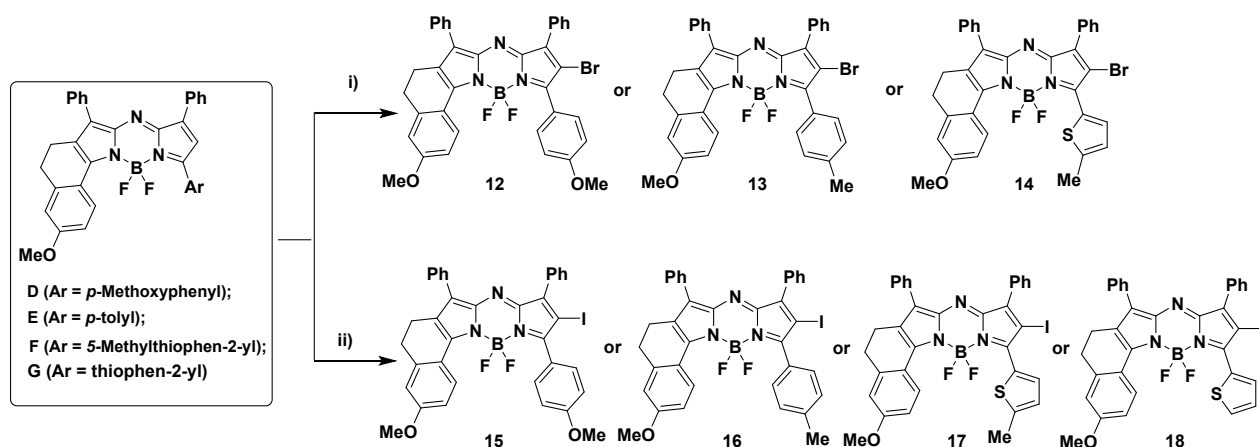
36  
37 **Scheme 2.** Synthesis of mono or dihalogenated aza-BODIPY photosensitizers.  
38  
39



Reagents and conditions: i) NIS (2.2 equiv), AcOH, DCM, r.t., 30 min; ii) NIS (1.0 equiv),  
AcOH, DCM, r.t., 30 min.

We finally paid our attention on conformationally restricted aza-BODIPY dyes with favorable long absorption maxima and greater absorption coefficient.<sup>51-52</sup> Various electron-donating aromatic and heteroaromatic groups were included to favor requirement of the deep tissue penetration. The non-symmetric dyes (**D~G**) were easily obtained.<sup>51-52</sup> Mono-brominated derivatives (**12~14**) and mono-iodinated species (**15~18**) were all prepared in excellent yields using the conditions shown in Scheme 3.

**Scheme 3.** Preparation of conformationally restricted aza-BODIPY photosensitizers.



Reagents and conditions: i) NBS (1.0 equiv), AcOH, DCM, r.t., 30 min; ii) NIS (1.0 equiv), AcOH, DCM, r.t., 30 min.

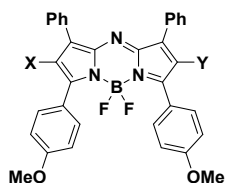
## 2.2. Spectroscopic, Photophysical Properties, and <sup>1</sup>O<sub>2</sub> Generation Efficiencies.

1  
2  
3  
4 The spectroscopic and photophysical properties of aza-BODIPY PSs were frequently  
5  
6  
7 evaluated in non-polar solvents in literatures.<sup>37-50</sup> The electronic absorption and  
8  
9  
10 fluorescence spectra of our aza-BODIPY dyes (**1~5**) were initially recorded in chloroform  
11  
12  
13 using compound **A** as reference dye and the spectroscopic data were collected in Table  
14  
15  
16  
17 1. The absorption maxima ( $\lambda_{\text{abs}}$ ) of halogenated aza-BODIPY displayed hypsochromic  
18  
19  
20 shift around 9 nm compared with the parent dye (compound **A** with  $\lambda_{\text{abs}}$  of 688 nm). In  
21  
22  
23 contrast, the emission maxima ( $\lambda_{\text{em}}$ ) of halogenated aza-BODIPY displayed only minor  
24  
25  
26 hypsochromic shift (2~5 nm) compared with the parent dye (compound **A** with  $\lambda_{\text{em}}$  of 725  
27  
28  
29 nm). The monohalogenated aza-BODIPYs presented minor decrease of absorption  
30  
31  
32 coefficient ( $\epsilon$  of 81,000, 97,000  $\text{M}^{-1}\text{cm}^{-1}$  for **3** and **4**, respectively) comparing with parent  
33  
34  
35 dye **A** ( $\epsilon$  of 99,000  $\text{M}^{-1}\text{cm}^{-1}$ ), whereas dihalogenated species ( $\epsilon$  of 77,000, 74,000  $\text{M}^{-1}\text{cm}^{-1}$   
36  
37  
38 for **1** and **2**, respectively) showed much decreased absorption coefficient. The mixed  
39  
40  
41 halogenated species (**5** with  $\epsilon$  of 76,000  $\text{M}^{-1}\text{cm}^{-1}$ ) behaved as dihalogenated species.  
42  
43  
44 Interestingly, while monobromination only led to trivial decline of fluorescence quantum  
45  
46  
47 yield ( $\Phi_f$ ) (comparing **3** with  $\Phi_f$  of 0.34 to **A** with  $\Phi_f$  of 0.36), dibrominated aza-BODIPY  
48  
49  
50 (**1**) revealed much decreased fluorescence quantum yield ( $\Phi_f = 0.17$ ). In contrast,  
51  
52  
53  
54  
55  
56  
57  
58  
59  
60

1  
2  
3  
4 monoiodo derivative (**4**) exhibited even smaller value of  $\Phi_f$  (0.08) than **1**. Diiodination  
5  
6  
7 resulted in much reduced fluorescence quantum yield ( $\Phi_f = 0.03$ ) as shown from the data  
8  
9  
10 of **2**. As expected, mixed halogenation (**5**) afforded significantly diminished fluorescence  
11  
12  
13 emission ( $\Phi_f = 0.07$ ). In PDT application, PSs were usually applied in aqueous  
14  
15  
16 environments. Due to the hydrophobic nature of aza-BODIPY dye, the photosensitization  
17  
18  
19 of aza-BODIPY type PS may behave significantly different in polar environment from non-  
20  
21  
22 polar solvent because of possible aggregation. We therefore examined the spectroscopic  
23  
24  
25 and photophysical properties of PSs in isopropanol (*i*PrOH), acetonitrile (CH<sub>3</sub>CN), *N,N*-  
26  
27  
28 dimethylformamide (DMF), as well as PBS buffer containing 1% Cremophor EL  
29  
30  
31 (CrEL)/1,2-propanediol (10:3, v:v). The absorption spectra of aza-BODIPY PSs in  
32  
33  
34 emulsified PBS buffer and in other polar solvents were shown in Fig. S1 (supporting  
35  
36  
37 information). The spectroscopic data in various polar environments were presented in  
38  
39  
40  
41  
42 Table S1 (supporting information). It can be found that in various solvents, all these  
43  
44  
45 halogenated compounds revealed intense Q-band with absorption maxima around  
46  
47  
48  
49  
50  
51  
52 665~685 nm, which falls into the body's therapeutic window (650~900 nm). In consistence  
53  
54  
55  
56 with the trend observed in chloroform, all PSs showed declined absorption coefficients  
57  
58  
59  
60

1  
2  
3 compared with the parent dye compound **A**. Notably, the absorption coefficients ( $\epsilon$ ) of all  
4  
5  
6  
7 dyes investigated revealed much declined values in PBS (34,000~59,000  $M^{-1}cm^{-1}$ )  
8  
9  
10 compared with those in organic media (59,300~105,000  $M^{-1}cm^{-1}$ ). Concurrently, the Full-  
11  
12  
13 Width Half-Maximum (FWHM) values in aqueous environment (87~90 nm) were  
14  
15  
16 significantly greater than those (56~67 nm) in organic solvents (Table S1).  
17  
18  
19  
20

21 **Table 1.** Photophysical data for the first round BODIPY photosensitizers.  
22  
23  
24



PS	$\lambda_{\text{abs}}$ (nm) <sup>a</sup>	$\epsilon$ ( $M^{-1} cm^{-1}$ ) <sup>a</sup>	$\lambda_{\text{em}}$	$\Phi_f$ <sup>a</sup>	rel. rate <sup>b</sup>	rel. rate <sup>c</sup>	rel. rate <sup>d</sup>	$\Phi_{\Delta}$ <sup>d</sup>
<b>A</b> (X=Y=H)	688	99000	725	0.36	0.28	0.30	0.04	0.02
<b>1</b> (X=Y=Br)	679	77000	720	0.17	4.5	1.9	0.36	0.14
<b>2</b> (X=Y=I)	679	74000	723	0.03	7.0	2.2	0.66	0.24
<b>3</b> (X=H; Y=Br)	679	81000	720	0.34	1.1	0.83	0.19	0.10
<b>4</b> (X=H; Y=I)	678	97000	721	0.08	7.3	2.4	1.3	0.52
<b>5</b> (X=Br; Y=I)	679	76000	720	0.07	6.8	2.3	0.65	0.29

25  
26  
27  
28  
29  
30  
31  
32  
33  
34  
35  
36  
37  
38  
39  
40  
41  
42  
43  
44  
45  
46  
47  
48  
49  
50  
51  
52  
53  
54  
55  
56  
57  
58  
59  
60

<sup>a</sup>In Chloroform; <sup>b</sup>Relative rate of degradation of DPBF to methylene blue in  $\text{PrOH}$ ;

<sup>c</sup>Relative rate of degradation of DPBF to methylene blue in PBS containing 1%

Cremophor EL (CrEL)/1,2-propanediol (10:3, v:v); <sup>d</sup>Measured in DMF using ZnPc ( $\Phi_{\Delta}$  =

0.56 in DMF) as standard.

1  
2  
3 To evaluate the photosensitizing abilities of these aza-BODIPY dyes, their singlet  
4 oxygen generation efficiencies were studied using 1,3-diphenylisobenzofuran (DPBF) as  
5  
6  
7  
8 oxygen generation efficiencies were studied using 1,3-diphenylisobenzofuran (DPBF) as  
9  
10  
11 singlet oxygen scavenger. The rate of photodegradation of this quencher was measured  
12  
13  
14 by monitoring the decrease in absorbance at 411 nm with time upon irradiation with light.  
15  
16  
17 Different from previous publications which evaluated photosensitizing efficiency  
18  
19  
20 frequently in non-polar solvent (*e.g.* toluene), we focused our investigations in polar  
21  
22  
23 environments (iPrOH, DMF, PBS buffer containing Cremophor EL) in order to find useful  
24  
25  
26 information for optimal PS. The photosensitizing capabilities of individual PS were carried  
27  
28  
29 out under irradiation with filtered light ( $\lambda > 590$  nm from halogen lamp with energy power  
30  
31  
32 of 90 mW/cm<sup>2</sup>). Time-dependent changes of absorption spectra of various aza-BODIPY  
33  
34  
35 dyes containing DPBF under light irradiation were shown in Fig. S2. The relative rates of  
36  
37  
38 degradation of DPBF monitored at 411 nm in iPrOH, DMF, PBS buffer containing 1%  
39  
40  
41 Cremophor EL (CrEL)/1,2-propanediol (10:3, v:v) were illustrated in Fig. S3 and the data  
42  
43  
44 calculated were collected in Table 1. From Fig. S2 and Fig. S3, it can be found that the  
45  
46  
47  
48  
49  
50  
51  
52 photosensitizing efficiencies of these PSs were solvent-dependent.  
53  
54  
55  
56  
57  
58  
59  
60

1  
2  
3  
4 As expected, the parent fluorescent dye **A** without any heavy atom in the molecule  
5  
6  
7 exhibited poor  $^1\text{O}_2$  generation ability in all solvents applied. In contrast, all halogenated  
8  
9  
10 aza-BODIPY PSs (**1**~**5**) revealed potent photosensitizing capability in  $\text{PrOH}$ . In  
11  
12  
13 consistent with previous reports,<sup>37-50</sup> dibrominated aza-BODIPY (**1**) or diiodinated aza-  
14  
15  
16 BODIPY (**2**) afforded potent photosensitization in  $\text{PrOH}$  and **2** was more effective than **1**.  
17  
18  
19 We also observed that **5** as mixed halogenated PS possessed nice photosensitizing  
20  
21  
22 ability as well ( $1 < 5 < 2$ ). Though monobromination enabled photosensitizing capability  
23  
24  
25 (see **3**) similar to the reference PS of methylene blue (**MB**), significant improvement of  
26  
27  
28 singlet oxygen generation was astonishingly found for monoiodo derivative (**4**) with up to  
29  
30  
31 7-fold rate relative to MB in  $\text{PrOH}$  for degradation of DPBF. It worth to note that monoiodo  
32  
33  
34 PS **4** exhibited much more potent photosensitizing ability than dibromo PS **1** and even  
35  
36  
37 more effective than mixed halogenated PS **5** and diiodo PS **2**. Such trend of halogenation  
38  
39  
40 effects were also observed in PBS buffer containing 1% Cremophor EL (CrEL)/1,2-  
41  
42  
43 propanediol (10:3, v:v) though degradation of DPBF was less efficient due to the  
44  
45  
46 hydrophobic nature of the aza-BODIPY PSs. Unexpectedly, when evaluation of  
47  
48  
49 photosensitizing capability was performed in dipolar aprotic solvent such as DMF or  
50  
51  
52  
53  
54  
55  
56  
57  
58  
59  
60

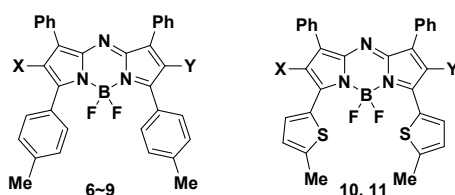
1  
2  
3 DMSO, it was found that obvious degradation of PS for halogenated aza-BODIPY  
4  
5  
6  
7 illustrated in the decrease of the absorbance of the NIR band was generally observed as  
8  
9  
10 shown in Fig. S2. To further evaluate the halogenation-related degradation, we selected  
11  
12  
13 ZnPc ( $\Phi_{\Delta}$  = 0.56 in DMF) as standard to compare the  $^1\text{O}_2$  generation efficiencies of PSs  
14  
15  
16 in DMF. In fact, dihalogenated aza-BODIPY (**1**, **2**) or mixed halogenated species (**5**)  
17  
18  
19 encountered significant degradation and afforded concurrently declined efficiency of  
20  
21  
22 production of  $^1\text{O}_2$  ( $\Phi_{\Delta}$  = 0.14 for **1**; 0.24 for **2**; 0.29 for **5**). While monobromo PS **3** ( $\Phi_{\Delta}$  =  
23  
24  
25 0.10) was weaker than those PSs with two halogen atoms, the monoiodinated aza-  
26  
27  
28 BODIPY (**4**) revealed excellent  $^1\text{O}_2$  production with  $\Phi_{\Delta}$  = 0.52 in DMF. We believed that  
29  
30  
31 the difference of photosensitizing ability among the aza-BODIPY PSs was amplified in  
32  
33  
34 DMF and such a solvent was used to evaluate other PSs in our subsequent modifications.  
35  
36  
37  
38  
39  
40

41  
42 The next round modification intended to inspect the generality of the trend observed  
43  
44  
45 above. To enable long absorption maxima, we installed *p*-tolyl moiety or 5-thiophenyl-2-  
46  
47  
48 yl group onto 3- and 5- positions of aza-BODIPY and the corresponding dyes were termed  
49  
50  
51 **B/C** respectively. The halogenated derivatives were listed in Table 2 and their properties  
52  
53  
54 were collected as well. It can be found that **B** derived PS series displayed slightly shorter  
55  
56  
57  
58  
59  
60

1  
2  
3 absorption maxima than **A** derived series whereas **C** derived PSs possessed longer  
4  
5  
6  
7 absorption maxima than compound **A** derived PSs as expected based on the electron-  
8  
9  
10 donating ability of the substituent. Unfortunately, though monoiodination resulted in  
11  
12  
13  
14 advantageous photosensitizing ability over monobromination, dibromination, or  
15  
16  
17 diiodination (comparing **9** with **8**, **6**, **7**; comparing **11** with **10**, Table 2), the  $^1\text{O}_2$  production  
18  
19  
20 quantum yields in DMF were relatively low for either **9** ( $\Phi_{\Delta}$  = 0.14) or **11** ( $\Phi_{\Delta}$  = 0.17). These  
21  
22  
23  
24 data implied that substituent on 3-/5- position of aza-BODIPY affected the  $^1\text{O}_2$  production  
25  
26  
27 and *p*-methoxyphenyl group was advantageous over *p*-tolyl or 5-thiophenyl-2-yl.

31 **Table 2.** Photophysical data for aza-BODIPY photosensitizers prepared according to

32  
33  
34  
35 Scheme 2.



46  
47  
48  
49  
50  
51  
52  
53  
54  
55  
56  
57  
58  
59  
60

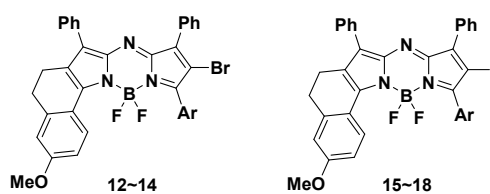
Entry	$\lambda_{\text{abs}}$ (nm) <sup>a</sup>	$\epsilon$ (M <sup>-1</sup> cm <sup>-1</sup> ) <sup>a</sup>	$\lambda_{\text{em}}$ (nm) <sup>a</sup>	$\Phi_{\text{f}}$ <sup>a</sup>	rel. rate <sup>b</sup>	$\Phi_{\Delta}$ <sup>b</sup>
<b>6</b> (X=Y=Br)	658	79900	685	0.04	0.22	0.10
<b>7</b> (X=Y=I)	662	92000	688	0.02	0.28	0.12
<b>8</b> (X=H; Y=Br)	658	83600	685	0.19	0.12	0.05
<b>9</b> (X=H; Y=I)	659	89600	690	0.04	0.26	0.14

10 (X=Y=I)	732	91300	768	0.07	0.36	0.14
11 (X=H; Y=I)	732	71700	766	0.11	0.32	0.17

<sup>a</sup>In chloroform; <sup>b</sup>Relative rate of degradation of DPBF and singlet oxygen quantum yield ( $\Phi_{\Delta}$ ) with reference to ZnPc ( $\Phi_{\Delta}$ = 0.56) in DMF.

**Table 3.** Photophysical data for aza-BODIPY photosensitizers prepared according to

Scheme 3.



Entry	$\lambda_{\text{abs}}(\text{nm})^a$	$\epsilon (\text{M}^{-1} \text{cm}^{-1})^a$	$\lambda_{\text{em}}(\text{nm})^a$	$\Phi_f^a$	rel. rate <sup>b</sup>	$\Phi_{\Delta}^b$
12 (Ar= <i>p</i> -MeOPh)	692	90300	724	0.44	0.17	0.08
13 (Ar= <i>p</i> -MePh)	682	104400	709	0.60	0.14	0.08
14 (Ar=5-Me-thiophen-2-yl)	714	73700	753	0.24	0.14	0.11
15 (Ar= <i>p</i> -MeOPh)	689	101300	725	0.14	1.2	0.51
16 (Ar= <i>p</i> -MePh)	682	110000	709	0.17	0.25	0.16
17 (Ar=5-Me-thiophen-2-yl)	716	76900	756	0.16	0.42	0.25
18 (Ar=thiophen-2-yl)	695	81500	740	0.16	0.37	0.19

<sup>a</sup>In chloroform; <sup>b</sup>Relative rate of degradation of DPBF and singlet oxygen quantum yield ( $\Phi_{\Delta}$ ) with reference to ZnPc ( $\Phi_{\Delta}$ = 0.56) in DMF.

The established advantageous  $^1\text{O}_2$  production with monoiodo aza-BODIPY derivatives shown in Tables 1 and 2 promoted us to apply various monoiodination on

1  
2  
3 conformationally-restricted aza-BODIPYs using 4,5-dihydro-7-methoxy-3-  
4  
5  
6 phenylbenzo[g]indole and 2-aryl-4-phenyl pyrrole to constitute the parent aza-BODIPY  
7  
8  
9  
10 core as shown in Scheme 3 in an attempt to further improve light penetration capability.<sup>51</sup>  
11  
12  
13  
14 Among the designed PSs, *p*-tolyl, *p*-methoxyphenyl, 5-methyl-thiophene-2-yl, and  
15  
16  
17 thiophene-2-yl were selected as the candidates of Ar in the pyrrole scaffold (The aza-  
18  
19  
20 BODIPYs constructed were termed as compounds **D**, **E**, **F**, and **G** respectively). Mono-  
21  
22  
23 brominated derivatives (**12**~**14**) and mono-iodinated species (**15**~**18**) were all examined  
24  
25  
26  
27 the photophysical properties and photosensitization capabilities and the results were  
28  
29  
30 collected in Table 3. As a general rule, the singlet oxygen quantum yields of  
31  
32  
33 monobrominated PSs (0.08~0.11) were inferior to monoiodinated PSs (0.16~0.51).  
34  
35  
36  
37  
38 Though thienyl (in **18** with  $\Phi_{\Delta}$  of 0.19) and 5-methyl-thiophene-2-yl (**17** with  $\Phi_{\Delta}$  of 0.25)  
39  
40  
41 led to long absorption maxima of the PSs, the photosensitizing capabilities were  
42  
43  
44 unfortunately suboptimal. *p*-Tolyl modified PSs (**13** and **16**) did not provide enough  $^1\text{O}_2$   
45  
46  
47  
48 generation quantum yields ( $\Phi_{\Delta}$  of 0.08, 0.16 respectively) and beneficial absorption  
49  
50  
51 maxima ( $\lambda_{\text{abs}}$  of 682 nm) over other conformationally-restricted PSs. Pleasantly, we  
52  
53  
54  
55 discovered that **15** carrying *p*-methoxyphenyl moiety possessed nice photosensitization  
56  
57  
58  
59  
60

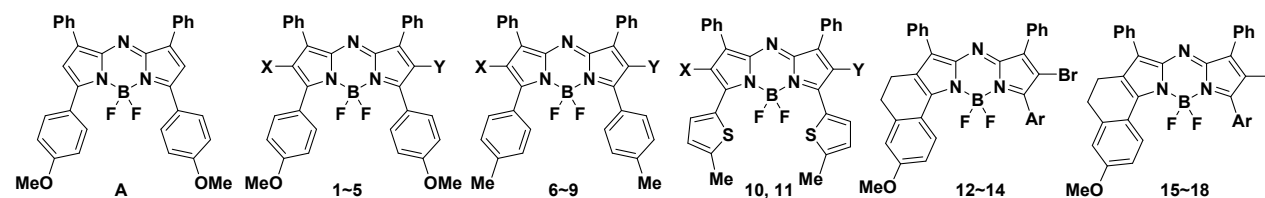
1  
2  
3 efficiency ( $\Phi_{\Delta}$  of 0.51), favorable absorption maximum ( $\lambda_{\text{abs}}$  of 689 nm), and absorption  
4  
5  
6  
7 coefficient ( $\epsilon$  of 101,300 M<sup>-1</sup>cm<sup>-1</sup>).  
8  
9

### 10 **2.3 Cytotoxicity assays.**

11  
12  
13  
14 The *in vitro* photodynamic activities of aza-BODIPYs in Cremophor emulsion were  
15  
16  
17 investigated against cervical carcinoma cell line (HeLa), breast cancer cell line (MCF-7),  
18  
19  
20 and colon carcinoma cell line (SW480) under irradiation with light > 590 nm using MTT  
21  
22  
23 assay with **Ce6** as reference PS (Table 4). Parallel assays without light irradiation were  
24  
25  
26  
27 also performed to determine the dark toxicity. As shown in Table 4, all the PSs have  
28  
29  
30 negligible dark toxicity up to 50  $\mu\text{M}$ . When irradiated with light dose of 54 J/cm<sup>2</sup>, IC<sub>50</sub>  
31  
32  
33 values of various PSs exhibited broad range of activity from micromolar to nanomolar  
34  
35  
36 level. In the series of aza-BODIPY **A** derived PSs, dibromo species **1** (**ADPM06**)  
37  
38  
39 possessed good light-induced toxicity (0.13~0.16  $\mu\text{M}$ ) for the investigated cell lines in  
40  
41  
42 consistence with the literature reports.<sup>39</sup> Diiodo PS **2** which efficiently generated high  
43  
44  
45 singlet oxygen in organic media was found to have unsatisfied potency with light toxicity  
46  
47  
48 around 1  $\mu\text{M}$ . Similarly, the mixed halogenated PS **5** presented suboptimal light toxicity  
49  
50  
51 around 0.5  $\mu\text{M}$ . To our surprise, monoiodo PS **4** displayed potent inhibition for all cell lines  
52  
53  
54  
55  
56  
57  
58  
59  
60

(up to 76 nM for HeLa cells) in consistent with efficient production of  $^1\text{O}_2$ . For **B** and **C** derived series wherein *p*-tolyl and 5-methylthiophene-2-yl were installed onto the 3,5-position of aza-BODIPY dye respectively, the monoiodo substituted photosensitizers (**9**, **11**) exhibited better efficacy than monobrominated (**8**) and dihalogenated (**6**, **7**, **10**) PSs in cell-based assays, even though the potency was relatively low. Among the conformationally restricted system, we were pleased to find that monoiodo derivatives (**15~18**) were generally more active than monobromo derivatives (**12~14**) and *p*-methoxyphenyl derived monoiodo PS (**15**) showed more potent inhibition than *p*-tolyl, 5-methylthiophene-2-yl, thiophene-2-yl derivatized PSs (**16**, **17**, **18** respectively).

**Table 4.** Photo and dark cytotoxicity of PSs in HeLa, MCF-7 and SW480 tumor cell lines.



PS	$\text{IC}_{50}$ ( $\mu\text{M}$ )					
	HeLa		MCF-7		SW480	
	0 J/cm <sup>2</sup>	54 J/cm <sup>2</sup>	0 J/cm <sup>2</sup>	54 J/cm <sup>2</sup>	0 J/cm <sup>2</sup>	54 J/cm <sup>2</sup>
<b>A (X=Y=H)</b>	>50	11.6±2.0	>50	9.4±1.3	>50	12.1±1.8

1							
2							
3							
4	1 (X=Y=Br)	>50	0.13±0.006	>50	0.15±0.01	>50	0.16±0.01
5							
6	2 (X=Y=I)	>50	0.59±0.12	>50	0.66±0.07	>50	1.3±0.11
7							
8							
9	3 (X=H; Y=Br)	>50	0.27±0.05	>50	0.35±0.06	>50	0.28±0.04
10							
11							
12	4 (X=H; Y=I)	>50	0.076±0.004	>50	0.10±0.01	>50	0.086±0.006
13							
14							
15	5 (X=Br; Y=I)	>50	0.31±0.05	>50	0.42±0.08	>50	0.53±0.06
16							
17							
18	6 (X=Y=Br)	>50	4.3±0.89	>50	1.5±0.20	>50	16.1±2.2
19							
20							
21	7 (X=Y=I)	>50	13.4±2.3	>50	5.3±0.43	>50	>25
22							
23							
24	8 (X=H; Y=Br)	>50	7.2±1.1	>50	2.6±0.18	>50	>25
25							
26							
27	9 (X=H; Y=I)	>50	2.6±0.46	>50	1.2±0.14	>50	12.4±2.0
28							
29							
30	10 (X=Y=I)	>50	>25	>50	16.4±2.9	>50	>25
31							
32							
33	11 (X=H; Y=I)	>50	15.6±3.2	>50	7.7±1.3	>50	20.6±3.2
34							
35							
36	12 (Ar= <i>p</i> -MeOPh)	>50	0.83±0.17	>50	4.5±0.41	>50	1.9±0.26
37							
38	13 (Ar= <i>p</i> -MePh)	>50	1.2±0.31	>50	8.1±1.3	>50	15.6±3.4
39							
40							
41	14 (Ar=5-Me-thiophen-2-yl)	>50	22.6±3.3	>50	>25	>50	>25
42							
43							
44	15 (Ar= <i>p</i> -MeOPh)	>50	0.081±0.01	>50	0.14±0.02	>50	0.12±0.01
45							
46							
47	16 (Ar= <i>p</i> -MePh)	>50	0.11±0.02	>50	0.41±0.06	>50	0.66±0.08
48							
49							
50	17 (Ar=5-Me-thiophen-2-yl)	>50	12.3±1.9	>50	16.6±3.8	>50	21.4±4.6
51							
52							
53	18 (Ar=thiophen-2-yl)	>50	0.46±0.09	>50	0.75±0.11	>50	0.83±0.14
54							
55							
56							
57							
58							
59							
60							

Ce6	>50	1.92±0.22	>50	3.4±0.29	>50	3.1±0.46
-----	-----	-----------	-----	----------	-----	----------

---

Through comparison of various aza-BODIPY PSs in solution-based and cell-based activities, we came to the conclusion that dihalogenation of aza-BODIPYs did not behave as expected to lead to potent PDT effect according to general trend of heavy atom effect.<sup>17,18,20</sup> Actually, two monoiodinated aza-BODIPY dyes (**4**, **15**) containing *p*-methoxyphenyl moiety among the investigated PSs offered excellent photosensitization and behaved as favorable PSs with intense long absorption, high phototoxicity and low dark toxicity. Therefore, our subsequent efforts focused on detailed studies of **4** as a nice example to confirm the advantage of monoiodination in comparison with known leading standard of **ADPM06** (compound **1**).

The cytotoxic effects under or without light irradiation for **4** and **1** against HeLa cells were shown in Fig. 2A and Fig. 2B, respectively. From Fig. 2A it can be concluded that **4** displayed better PDT activity than **1** over the investigated concentration range. As shown in Fig. 2B, though both PSs exhibited minimal dark toxicity against HeLa cells without

light irradiation, the cell viability evaluations clearly suggested the dibromination led to greater dark toxicity than monoiodination.

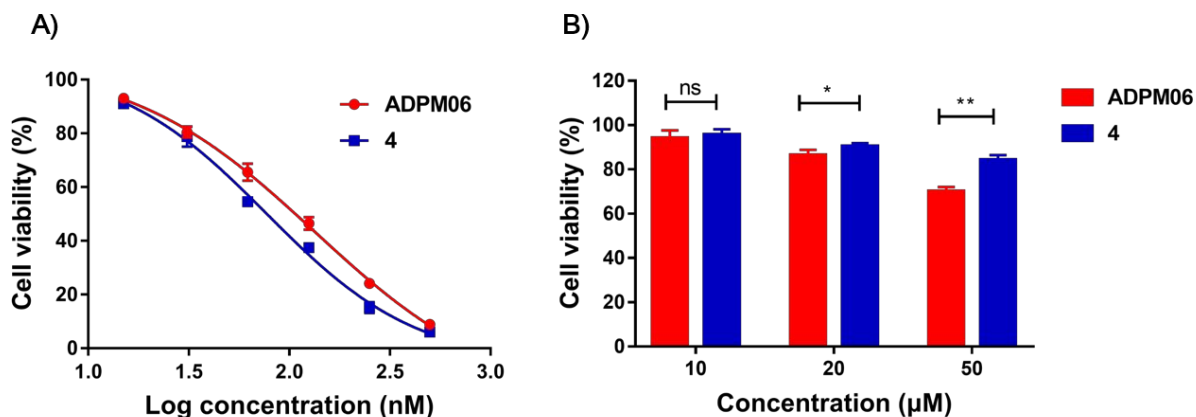


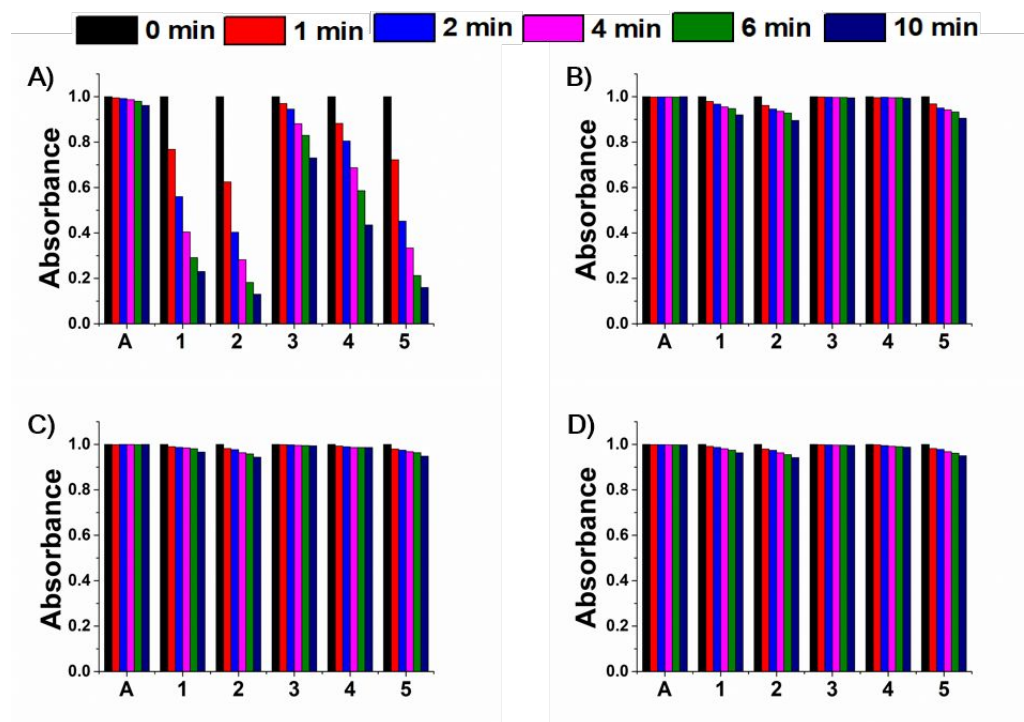
**Figure 2.** Photo toxicity (A) and dark toxicity (B) of photosensitizers **4** and **ADPM06** against HeLa cells. Light dose: 54 J/cm<sup>2</sup>,  $\lambda > 590$  nm. \* $p < 0.05$ , \*\* $p < 0.01$ .

To further investigate the PDT behavior of **4**, light dose-dependent phototoxicity assays were performed and the results were displayed in Fig. S4. From Fig. S4, we were pleased to find that **4** exhibited light dose-dependent antitumor activity against HeLa cells and much greater cell killing ability was achieved by **4** under stronger exposure of light irradiation.

#### 2.4. Photostability and thermal stability studies.

1  
2  
3  
4 Upon evaluation of photosensitivity, we have noticed that some PSs encountered  
5  
6  
7 degradation during light irradiation (Fig. S2). We suspected that the observed *in vitro*  
8  
9  
10 efficacy may significantly rely on the stability of PS. To investigate the photostability  
11  
12  
13 behavior comprehensively and establish the relationship between the stability and  
14  
15  
16 potency, we selected A-derived series and monitored the absorbance of PSs in *N,N*-  
17  
18 dimethylformamide (DMF), acetonitrile (CH<sub>3</sub>CN), isopropanol (iPrOH) and PBS buffer  
19  
20  
21 containing 1% Cremophor EL (CrEL)/1,2-propanediol (10:3, v:v) respectively under  
22  
23  
24 irradiation with light ( $\lambda > 590$  nm, light power: 90 mW/cm<sup>2</sup>). As shown in Fig. 3, all PSs  
25  
26  
27 encountered obvious degradation in DMF under irradiation and followed the trend of  
28  
29  
30 stability as **A > 3 > 4 > 1 > 5 > 2**. Same trend was also found in other solvent *e.g.* CH<sub>3</sub>CN,  
31  
32  
33 iPrOH, or emulsified PBS buffer, however, the degradation of PS was insignificant.  
34  
35  
36 Meanwhile, the thermal stabilities in the dark without irradiation in CH<sub>3</sub>CN and emulsified  
37  
38  
39 PBS buffer (containing minimum amount of detergent) were investigated as well and the  
40  
41  
42 results were displayed in Fig. S5. Slow degradation of PS in the dark was discovered for  
43  
44  
45 all dyes investigated both in CH<sub>3</sub>CN and emulsified PBS buffer and followed the same  
46  
47  
48 trend as light-induced degradation (Fig. 3). As demonstrated in Fig. 3 and Fig. S5,  
49  
50  
51  
52  
53  
54  
55  
56  
57  
58  
59  
60

1  
2  
3 monohalogenated PSs possessed much better stability than dihalogenated and mixed  
4  
5  
6  
7 halogenated PSs. Therefore, the stability studies may provide a plausible explanation for  
8  
9  
10 the observed potent PDT effect of 4.  
11  
12



38 **Figure 3.** Normalized absorbance-irradiation time histogram of dyes and photosensitizers  
39 in different solvents: (A) DMF; (B) CH<sub>3</sub>CN; (C) *i*PrOH; (D) PBS buffer containing 0.01%  
40  
41 Cremophor EL (CrEL)/1,2-propanediol (10:3, v:v). Light power: 90 mW/cm<sup>2</sup> ( $\lambda > 590$  nm).  
42  
43  
44  
45

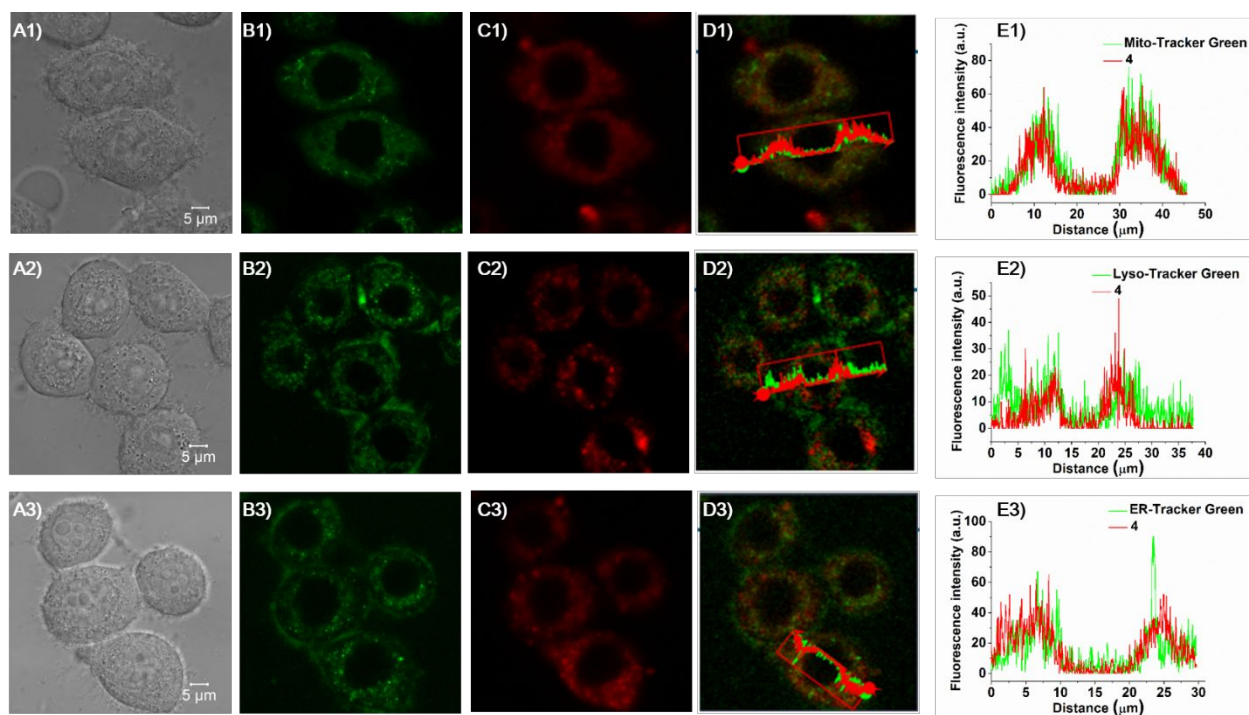
## 46 2.5. Subcellular localization.

47  
48  
49  
50  
51 The subcellular localization of photosensitizer is critical for photodynamic effect and  
52  
53  
54 plays critical role for the mode of cell death.<sup>5</sup> Since singlet oxygen has short half-life (~3.5  
55  
56  
57  
58  
59  
60

1  
2  
3  $\mu\text{s}$ ) and limited diffusion distance ( $< 0.02 \mu\text{m}$ ),<sup>53-55</sup> the sites where the photosensitizers  
4  
5  
6  
7 accumulated in tumor cells coincide with the photo-damaged cellular structures. Actually,  
8  
9  
10 some examples of subcellular-targeted photosensitizers were reported and it was well-  
11  
12  
13 known that subcellular localization of photosensitizers could strongly affect the cell death  
14  
15  
16  
17 pathways.<sup>56</sup> Mitochondria perform critical cellular functions in regulating multiple signaling  
18  
19  
20  
21 cascade reactions, such as energy production, intrinsic apoptotic mediated by caspase  
22  
23  
24 9/caspase 3 pathway and cell cycle regulation, thus acting as a crucial target for PDT.<sup>57</sup>  
25  
26  
27  
28 Localization of photosensitizers in mitochondria can cause *in situ* damage, maximize the  
29  
30  
31 killing effect of the photosensitizer, lead to the destruction of the cells' energy supply  
32  
33  
34  
35 system and ultimately cell death.<sup>58-60</sup>  
36  
37

38 To investigate the subcellular localization behavior of **4**, laser confocal microscopy  
39  
40  
41 studies were performed on HeLa cells incubated with **4** together with commercially  
42  
43  
44 available organelle-targeted dyes (Mito Tracker Green FM, Lyso Tracker Green, or ER  
45  
46  
47 Tracker Green) and their co-localization patterns were displayed in Fig. 4. The overlapped  
48  
49  
50  
51 images indicated that **4** revealed good overlap with Mito Tracker Green FM (Fig. 4D1/E1),  
52  
53  
54  
55 as well as partial colocalization with Lyso Tracker Green (Fig. 4D2/E2) and ER Tracker  
56  
57  
58  
59  
60

1  
2  
3  
4 Green (Fig. 4D3/E3), indicating that **4** was mainly localized in mitochondria, and  
5  
6 distributed a part in endoplasmic reticulum and lysosomes. The subcellular localization  
7  
8  
9  
10 studies of **4** may afford reasonable explanation for its excellent phototoxicity.  
11  
12



13  
14  
15  
16  
17  
18  
19  
20  
21  
22  
23  
24  
25  
26  
27  
28  
29  
30  
31  
32  
33  
34  
35  
36  
37  
38 **Figure 4.** Subcellular location of **4** in HeLa cells at 10  $\mu\text{M}$  for 2 h: (A1, A2, A3) bright field;  
39  
40 (B1) fluorescence of Mito Tracker Green (250 nM); (B2) fluorescence of Lyso Tracker  
41  
42 Green (160 nM); (B3) fluorescence of ER Tracker Green (2  $\mu\text{M}$ ); (C1, C2, C3) the  
43  
44 corresponding red fluorescence of **4**; (D1, D2, D3) the corresponding superimposed  
45  
46 images of organelle trackers and **4**; (E1, E2, E3) Luminescence intensity profiles of  
47  
48 regions of interest (ROI) across HeLa cells in (D1, D2, D3) respectively. Scale bar: 5  $\mu\text{m}$ .  
49  
50  
51  
52  
53

## 54 2.6. Investigation on cell death pathway.

55  
56  
57  
58  
59  
60

1  
2  
3 Apoptosis is an important manner of cell death after illumination during photodynamic  
4 therapy.<sup>61,62</sup> In early apoptotic cells, phosphatidylserine exposes to the outside of the cell  
5  
6 membrane, which can bind to Annexin-V with high affinity. Propidium iodide (PI) is able  
7  
8 to stain nucleus of late apoptotic and necrotic cells. Since **4** located majorly in  
9  
10 mitochondria, we were looking forward to know whether apoptosis is the major way of cell  
11  
12 death. Therefore, Annexin V-FITC/PI double staining flow cytometry assay was  
13  
14 conducted to evaluate the effect caused by **4** in HeLa cells. As is shown in Fig. 5, no  
15  
16 obvious apoptotic cells was detected in control experiment wherein photosensitizers and  
17  
18 light irradiation were not treated (Fig. 5A). When the cells were incubated with 40 nM of  
19  
20 **4** and irradiated with 54 J/cm<sup>2</sup> of light ( $\lambda > 590$  nm), the proportion of apoptotic cells was  
21  
22 about 20.99% (Fig. 5B). Using 200 nM of PS and exposed to 27 J/cm<sup>2</sup> of light increased  
23  
24 the apoptosis to 35.44% (Fig. 5C). Upon increment of light dose to 54 J/cm<sup>2</sup>, the apoptosis  
25  
26 reached to 89.64% (Fig. 5D). These results demonstrated that **4** induced major death of  
27  
28 cells through early/late apoptosis and also resulted in some necrosis under light  
29  
30 irradiation.  
31  
32  
33  
34  
35  
36  
37  
38  
39  
40  
41  
42  
43  
44  
45  
46  
47  
48  
49  
50  
51  
52  
53  
54  
55  
56  
57  
58  
59  
60

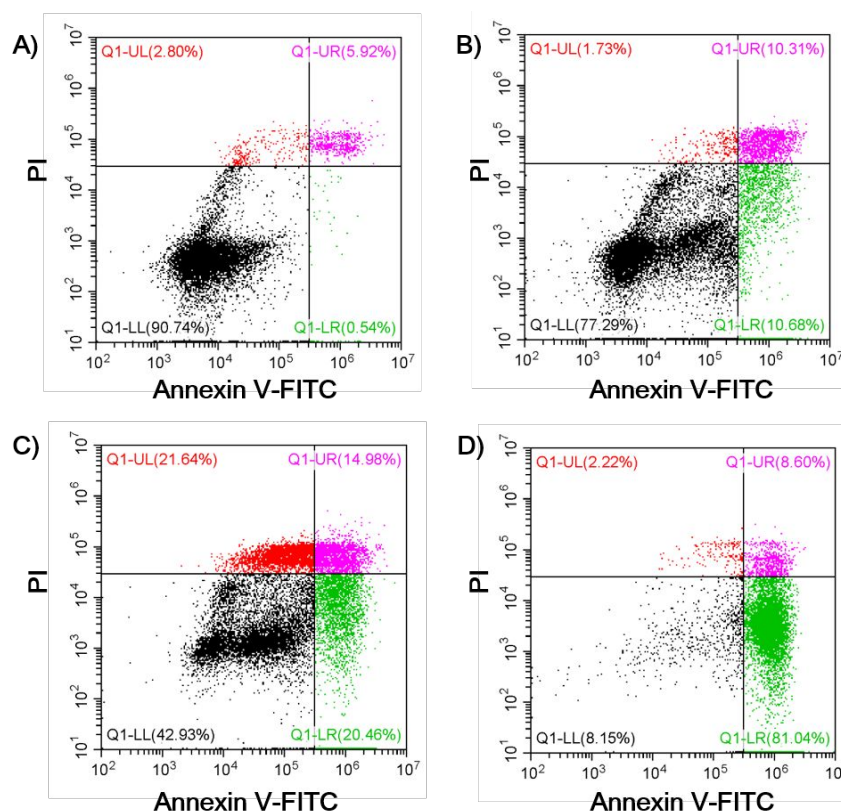


**Figure 5.** Flow cytometric evaluations of **4** on cellular apoptosis in HeLa cells: (A) Control without PS and light irradiation; (B) Treatment with 40 nM of **4** for 2 h and irradiated with light dose of 54 J/cm<sup>2</sup>; (C) Incubation with 200 nM of **4** for 2 h and irradiated with light dose of 27 J/cm<sup>2</sup>; (D) Incubation with 200 nM of **4** for 2 h and irradiated with light dose of 54 J/cm<sup>2</sup>; LL (lower left quadrant): Annexin V (-) PI (-), survival cell; LR (lower right quadrant): Annexin V (+) PI (-), early apoptotic cells; UR (upper right quadrant): Annexin V (+) PI (+), late apoptotic or necrotic cells; UL (upper left quadrant): Annexin V (-) PI (+), dead cells.

## 2.7. Intracellular ROS production.

1  
2  
3  
4        Photosensitizers eradicate tumor cells by reactive oxygen species (ROS) produced by  
5  
6  
7 type I and/or type II reactions, thus the produced ROS level can reflect the therapeutic  
8  
9  
10 effect in photodynamic reactions.<sup>63,64</sup> We measured the production of ROS inside HeLa  
11  
12  
13 cells using commercially available 2',7'-dichlorodihydrofluorescein diacetate (H<sub>2</sub>DCFDA)  
14  
15  
16 as a probe. HeLa cells were incubated with various concentrations of **4** followed by  
17  
18  
19 H<sub>2</sub>DCFDA and then subjected to light irradiation. As shown in Fig. S6A–E, while  
20  
21  
22 intracellular ROS generation reflected by the green fluorescence emission exhibited a  
23  
24  
25 concentration-dependent manner ranging from 0.004 to 2.5  $\mu$ M, the ROS level in the dark  
26  
27  
28 remained low. The clear difference between light irradiation and dark conditions was  
29  
30  
31 easily caught in Fig. 6A wherein relative intensities of fluorescence emission were  
32  
33  
34 compared. Moreover, to verify the accuracy of the results, the ROS levels were also  
35  
36  
37 measured using the microplate reader method (Fig. 6B). The increment of fluorescence  
38  
39  
40 was in consistent with the results observed from confocal fluorescence studies. At a  
41  
42  
43 concentration of 2.5  $\mu$ M of **4**, the ROS level inside HeLa cells was about 77-fold than that  
44  
45  
46 of the dark control measured by microplate reader.  
47  
48  
49  
50  
51  
52  
53  
54  
55  
56  
57  
58  
59  
60

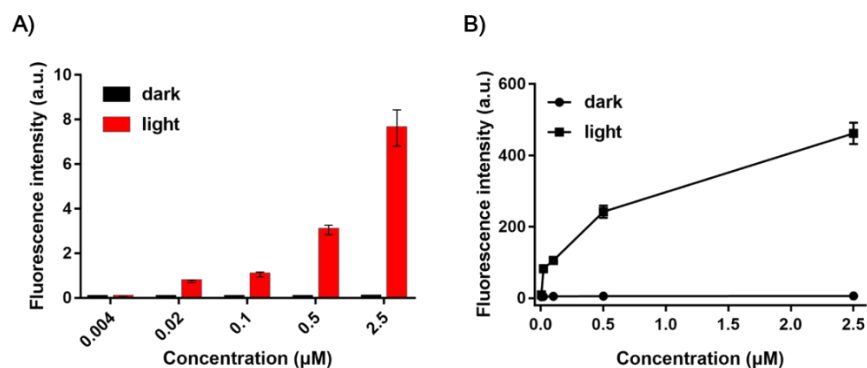


**Figure 6.** Determination of **4** induced intracellular reactive oxygen species. (A) Relative fluorescence intensities in Fig.S6. (B) Relative fluorescence intensities measured by microplate reader. Light dose: 54 J/cm<sup>2</sup> ( $\lambda > 590$  nm).

## 2.8 *In vivo* fluorescence imaging and distribution in organs for **4**.

One of the advantages of our **4** is that the PS possesses NIR fluorescence and allows *in vivo* imaging as a convenient tool to study the distribution and clearance of the PS. The *in vivo* fluorescence images of **4** were collected after intravenous injection through the tail vein at a dose of 2 mg/kg. As displayed in Fig. S7A, **4** quickly distributed to the whole-body inside living mice and gradually cleared from the major organs over 10 h, which indicated the fast uptake and reasonable clearance rate. To further characterize the distribution of **4**, mice injected with **4** were executed at various time period and imaging of major organs dissected were performed (Fig. S7B). The organ distribution studies

1  
2  
3  
4 turned out that the peak fluorescence intensities for liver, lungs, spleen, and kidneys were  
5  
6  
7 within 1 h, while the tumor and heart accumulated PS to the maximum degree around 3  
8  
9  
10 h. The clearance in major organs was found to be faster than that in tumor and reasonable  
11  
12  
13 amount of PS was retained in tumor site (Fig. S7C).  
14  
15  
16

### 17 **2.9. *In vivo* response to 4-mediated PDT under single time light irradiation.**

18  
19  
20

21 To further validate the anti-tumor effect of **4** in animals, HeLa tumor-bearing nude mice  
22  
23 were used for *in vivo* efficacy studies. **ADPM06** (**1** in this study) as an advanced PS of  
24  
25 aza-BODIPY type was selected for comparison and commercially **Ce6** was used as  
26  
27 porphyrin type PS standard. In most reported cases, the good *in vivo* anti-tumor  
28  
29 treatments were achieved through multiple PDT treatments.<sup>65</sup> In this paper, to testify the  
30  
31 effectiveness of PSs and reveal anti-tumor effect of our PS, only a single time irradiation  
32  
33 with light from a 75 W halogen lamp ( $\lambda > 590$  nm) was adopted after initial investigation.  
34  
35 All photosensitizers were dosed with 2 mg/kg and light energy of 54 J/cm<sup>2</sup> ( $\lambda > 590$  nm)  
36  
37 were applied for irradiation. The control groups were also exposed to 54 J/ cm<sup>2</sup> ( $\lambda > 590$   
38  
39 nm) light irradiation wherein physiological saline was used as control. As shown in Fig. 7  
40  
41 (A–C), the control group faced relative fast tumor growth with extend time period. The  
42  
43  
44  
45  
46  
47  
48  
49  
50  
51  
52  
53  
54  
55  
56  
57  
58  
59  
60

1  
2  
3 commercial PS of **Ce6** exhibited insignificant tumor-inhibition after irradiation with 54  
4  
5  
6  
7 J/cm<sup>2</sup> of light. In contrast, **ADPM06** retarded tumor growth significantly in accordance with  
8  
9  
10 the reported anti-tumor ability.<sup>40</sup> To our delight, **4** was discovered to have the best efficacy  
11  
12  
13 with dramatically delayed tumor growth ( $p < 0.001$  compared with **ADPM06** group) under  
14  
15  
16 the situation wherein only a single light irradiation was performed at beginning of the  
17  
18  
19 investigation and no other treatment was provided over the investigated time period. Body  
20  
21  
22 weight measurements suggested that **4** and **ADPM06** group all performed steady  
23  
24  
25 increase which is better than control group. However, **Ce6** group showed body loss at the  
26  
27  
28 late stage of the investigated period and the control group encountered great body weight  
29  
30  
31  
32 decrease along with time extended (Fig. 7D).  
33  
34  
35  
36  
37  
38  
39  
40  
41  
42  
43  
44  
45  
46  
47  
48  
49  
50  
51  
52  
53  
54  
55  
56  
57  
58  
59  
60

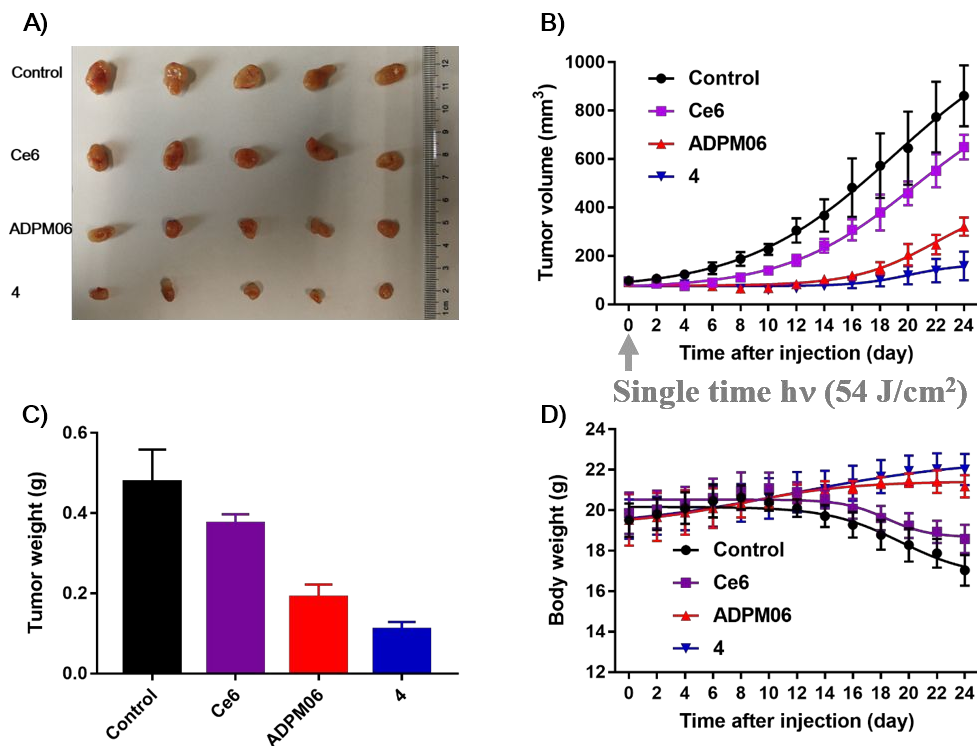


**Figure 7.** Evaluation of tumor growth inhibition in HeLa-tumor bearing xenograft model mediated by PDT. (A) Dissected tumor images after 24 days; (B) Tumor growth curves; (C) Isolated tumor weight; (D) Nude mice body weight change curves. Light irradiation was only performed at day 0 for all groups with light dose of 54 J/cm<sup>2</sup> ( $\lambda > 590$  nm from a 75 W halogen lamp with energy power of 90 mW/cm<sup>2</sup> for 10 min) on the tumor site without anaesthetization.

### 3. CONCLUSION

In summary, through systematic evaluation of halogen substitution on aza-BODIPY, we have found that moniodo-derived aza-BODIPYs possess better efficacy than

1  
2  
3 monobromo, dibromo-, diiodo-, or mixed halogenated aza-BODIPY PSs. We have  
4  
5  
6 identified monoiodinated aza-BODIPY dyes (**4**, **15**) containing *p*-methoxyphenyl moiety  
7  
8  
9 as efficient NIR aza-BODIPY type PSs. **4** with intense NIR absorption, high  $^1\text{O}_2$   
10  
11 generation capability, low dark-toxicity and good thermal/photo stability was selected to  
12  
13 investigate cell-death pathway, subcellular distribution, *in vitro* ROS generation to provide  
14  
15 the key information for such a NIR PS. *In vivo* whole-body fluorescence imaging and *ex*  
16  
17  
18 *vivo* organ distribution studies suggested that **4** behaved as very nice NIR PS with  
19  
20 reasonable clearance and tumor accumulation. *In vivo* efficacy studies indicated that even  
21  
22 with low drug dose of 2 mg/kg and light dose of 54 J/cm<sup>2</sup> with single time irradiation, the  
23  
24 tumor growth was dramatically inhibited without causing body weight loss. Our non-  
25  
26 porphyrin PS **4** possessed advantages of ideal PS and led to better efficacy than **ADPM06**  
27  
28 and **Ce6**. We hope that through systemic investigations examined, we have demonstrated  
29  
30 that monoiodo aza-BODIPY PS provides overall better PDT behavior and improved  
31  
32 stability and dark toxicity over dibromo, diiodo, and mixed halogenated PS. Our studies  
33  
34 may encourage scientific community to open a new way to develop powerful NIR PS.  
35  
36  
37  
38  
39  
40  
41  
42  
43  
44  
45  
46  
47  
48  
49  
50  
51  
52  
53  
54

#### 55 56 **4. EXPERIMENTAL SECTION**

#### 4.1. Chemistry and experimental instruments.

All chemical reagents were of analytical grade and purchased from commercial sources and used without further purification. Anhydrous solvents were acquired by standard methods prior to use. TLC analysis was performed on silica gel plates GF254 and chromatography was carried out on 200–300 mesh silica gel (Qingdao Haiyang Chemical, China).  $^1\text{H}$ -NMR spectra were measured on a Varian Model Mercury 400 MHz or 600 MHz spectrometer.  $^{13}\text{C}$ -NMR spectra were performed on a Varian Model Mercury 150 MHz spectrometer. Chemical shifts ( $\delta$ ) were expressed in ppm (parts per million) and coupling constant ( $J$ ) were recorded in hertz (Hz). HRMS (high resolution mass spectrometry, DART positive) spectra were obtained on Thermo Fisher Scientific LTQ FT Ultra. Purity of the compounds were analyzed using high-performance liquid chromatography (HPLC) (Agilent Technologies 1200 Infinity) at 1 mL/min on a C18 column (Agilent 5 HC-C18, 250  $\times$  4.6 mm). Compounds were first dissolved in THF/ $\text{CH}_3\text{CN}$  (1:9, volume ratio) and pure  $\text{CH}_3\text{CN}$  was used as the mobile phase. All compounds displayed purity of more than 95%.

1  
2  
3 The pyrrole derivatives and aza-BODIPY dyes (**A~G**) were synthesized according to  
4  
5  
6  
7 the procedure reported.<sup>51</sup>  
8  
9

10 *General procedure to synthesize non-symmetric aza-BODIPY dyes:*

11  
12  
13  
14 The first molecular pyrrole derivative (0.1 mmol) was added to glacial acetic acid (1  
15  
16  
17 mL), then sodium nitrite (6.9 mg, 0.1 mmol) was slowly added and stirred for 15 min. The  
18  
19  
20  
21 color of the solution changed from colorless to brown, then to green, and finally brown  
22  
23  
24 was observed. Then, the second pyrrole derivative (0.1 mmol) was added, followed by  
25  
26  
27  
28 acetic anhydride (0.4 ml), the reaction mixture immediately turned green, stirring was  
29  
30  
31 continued for 30 min at room temperature, then warmed to 80 °C for 30 min. The reaction  
32  
33  
34  
35 was monitored by TLC until the complete consumption of the starting material. The  
36  
37  
38  
39 reaction solution was cooled to room temperature, quenched by the addition of ice water,  
40  
41  
42 the precipitated blue dye was filtered, and the filter cake was rinsed with water and dried.  
43  
44  
45  
46 The filter cake was chromatographed on a neutral alumina column, dichloromethane was  
47  
48  
49 used as an eluent, and the solvent was evaporated to dryness.  
50  
51

52 The resulted residue was dissolved in 1,2-dichloroethane, triethylamine (0.24 ml) was  
53  
54  
55  
56 added, then a solution of boron trifluoride diethyl ether (0.24 ml) was added and reacted  
57  
58  
59  
60

1  
2  
3 at room temperature for 30 min and then 80 °C for 30 min. The reaction solution was  
4  
5  
6 cooled to room temperature, crushed ice was added, extracted with CH<sub>2</sub>Cl<sub>2</sub> and water,  
7  
8  
9  
10 and the organic layer was combined, washed with saturated brine, dried over anhydrous  
11  
12  
13 sodium sulfate. The obtained organic phase was concentrated and purified by column  
14  
15  
16 chromatography with CH<sub>2</sub>Cl<sub>2</sub> as eluent. The product was recrystallized from  
17  
18  
19  
20  
21 CH<sub>2</sub>Cl<sub>2</sub>/hexane.  
22

23  
24 *General procedure to synthesize dihalogenated aza-BODIPY photosensitizers:*  
25

26  
27  
28 Aza-BODIPY dye (0.036 mmol) was dissolved in CH<sub>2</sub>Cl<sub>2</sub> (6 ml), acetic acid (2 ml) was  
29  
30  
31 added, followed by the addition of NBS or NIS (0.079 mmol) and allowed to react at room  
32  
33  
34 temperature for 30 min. The mixture were washed with sodium sulfate aqueous and  
35  
36  
37 CH<sub>2</sub>Cl<sub>2</sub> for three times, and the organic phases were combined and separated by column  
38  
39  
40 chromatography with CH<sub>2</sub>Cl<sub>2</sub> as eluent. The product was recrystallized from  
41  
42  
43  
44  
45 CH<sub>2</sub>Cl<sub>2</sub>/petroleum ether (1/1) to give the final product. For **5**, **4** was used as starting  
46  
47  
48 material.  
49

50  
51  
52 *BF<sub>2</sub> Chelate of [4-bromo-5-(4-methoxyphenyl)-3-phenyl-1H-pyrrol-2-yl][4-bromo-5-(4-*  
53  
54  
55 *methoxyphenyl)-3-phenylpyrrol-2-ylidene]amine (1)*,<sup>38</sup> coppery solid, yield 91.3%. <sup>1</sup>H  
56  
57

1  
2  
3  
4 NMR (400 MHz, CDCl<sub>3</sub>) δ 7.84 (dd, *J* = 6.9, 2.8 Hz, 4H), 7.80 – 7.73 (m, 4H), 7.43 (dd, *J*  
5  
6  
7 = 5.2, 2.0 Hz, 6H), 7.01 – 6.94 (m, 4H), 3.85 (s, 6H).  
8  
9

10  
11 *BF<sub>2</sub> Chelate of [4-iodo-5-(4-methoxyphenyl)-3-phenyl-1H-pyrrol-2-yl][4-iodo-5-(4-*  
12  
13 *methoxyphenyl)-3-phenylpyrrol-2-ylidene]amine (2)*, coppery solid, yield 90.4%. <sup>1</sup>H NMR  
14  
15 (400 MHz, CDCl<sub>3</sub>) δ 7.82 – 7.76 (m, 4H), 7.70 (d, *J* = 8.5 Hz, 4H), 7.43 (t, *J* = 3.3 Hz, 6H),  
16  
17  
18 7.01 – 6.95 (m, 4H), 3.86 (s, 6H). <sup>13</sup>C NMR (151 MHz, CDCl<sub>3</sub>) δ 161.60, 160.47, 147.92,  
19  
20  
21 145.02, 132.41, 131.96, 130.73, 129.40, 127.86, 123.31, 113.47, 83.04, 55.29. HRMS  
22  
23  
24 (DART) *m/z*. 809.0121 [M + H]<sup>+</sup>, calcd for C<sub>34</sub>H<sub>25</sub>BF<sub>2</sub>I<sub>2</sub>N<sub>3</sub>O<sub>2</sub> 809.0128.  
25  
26  
27  
28  
29  
30

31  
32 *BF<sub>2</sub> Chelate of [4-bromo-3-phenyl-5-(4-tolyl)-1H-pyrrol-2-yl][4-bromo-3-phenyl-5-(4-*  
33  
34 *tolyl)-pyrrol-2-ylidene]amine (6)*, coppery solid, yield 93.1%. <sup>1</sup>H NMR (400 MHz, CDCl<sub>3</sub>)  
35  
36 δ 7.90 – 7.83 (m, 4H), 7.66 (d, *J* = 8.0 Hz, 4H), 7.45 (dd, *J* = 5.0, 1.9 Hz, 6H), 7.28 (d, *J*  
37  
38 = 8.4 Hz, 4H), 2.41 (s, 6H). <sup>13</sup>C NMR (151 MHz, CDCl<sub>3</sub>) δ 157.73, 143.61, 142.10, 140.71,  
39  
40  
41  
42 130.13, 130.01, 129.72, 128.91, 128.16, 127.37, 125.96, 109.64, 21.08. HRMS (DART)  
43  
44  
45  
46  
47  
48  
49 *m/z*. 681.0495 [M + H]<sup>+</sup>, calcd for C<sub>34</sub>H<sub>25</sub>BBr<sub>2</sub>F<sub>2</sub>N<sub>3</sub> 681.0507.  
50  
51

52  
53 *BF<sub>2</sub> Chelate of [4-iodo-3-phenyl-5-(4-tolyl)-1H-pyrrol-2-yl][4-iodo-3-phenyl-5-(4-tolyl)-*  
54  
55 *pyrrol-2-ylidene]amine (7)*, coppery solid, yield 87.1%. <sup>1</sup>H NMR (400 MHz, CDCl<sub>3</sub>) δ 7.78  
56  
57  
58  
59  
60

1  
2  
3 (dd,  $J = 6.8, 2.9$  Hz, 4H), 7.56 (d,  $J = 7.9$  Hz, 4H), 7.42 (t,  $J = 3.3$  Hz, 6H), 7.25 (s, 4H),  
4  
5  
6  
7 2.39 (s, 6H).  $^{13}\text{C}$  NMR (151 MHz,  $\text{CDCl}_3$ )  $\delta$  148.05, 141.09, 131.88, 130.71, 130.31,  
8  
9  
10 129.47, 128.69, 128.14, 127.88, 21.71. HRMS (DART)  $m/z$ : 777.0237  $[\text{M} + \text{H}]^+$ , calcd for  
11  
12  
13  
14  $\text{C}_{34}\text{H}_{25}\text{BF}_2\text{I}_2\text{N}_3$  777.0230.

15  
16  
17 *BF<sub>2</sub> Chelate of [4-iodo-5-(5-methylthiophen-2-yl)-3-phenyl-1H-pyrrol-2-yl][4-iodo-5-(5-*  
18  
19  
20 *methylthiophen-2-yl)-3-phenylpyrrol-2-ylidene]amine (10)*, coppery solid, yield 91.5%.  $^1\text{H}$   
21  
22  
23  
24 NMR (400 MHz,  $\text{CDCl}_3$ )  $\delta$  7.86 (d,  $J = 3.8$  Hz, 2H), 7.69 (dd,  $J = 6.6, 3.0$  Hz, 4H), 7.42 –  
25  
26  
27 7.35 (m, 6H), 6.90 (d,  $J = 3.0$  Hz, 2H), 2.58 (s, 6H).  $^{13}\text{C}$  NMR (151 MHz,  $\text{CDCl}_3$ )  $\delta$  151.87,  
28  
29  
30  
31 147.77, 147.43, 144.62, 135.25, 131.43, 130.19, 128.63, 128.45, 127.12, 126.22, 82.30,  
32  
33  
34  
35 15.09. HRMS (DART)  $m/z$ : 788.9361  $[\text{M} + \text{H}]^+$ , calcd for  $\text{C}_{30}\text{H}_{21}\text{BF}_2\text{I}_2\text{N}_3\text{S}_2$  788.9358.

36  
37  
38 *General procedure to synthesize monohalogenated aza-BODIPY photosensitizers:*  
39

40  
41  
42 Aza-BODIPY dye (0.036 mmol) was dissolved in  $\text{CH}_2\text{Cl}_2$  (6 ml), acetic acid (2 ml) was  
43  
44  
45 added, followed by the addition of NBS or NIS (0.036 mmol) and allowed to react at room  
46  
47  
48 temperature for 30 min. The mixture were extracted with sodium sulfate aqueous and  
49  
50  
51  
52  $\text{CH}_2\text{Cl}_2$  for three times, and the organic phases were combined and separated by column  
53  
54  
55  
56  
57  
58  
59  
60

1  
2  
3 chromatography with CH<sub>2</sub>Cl<sub>2</sub> as eluent. The product was recrystallized from  
4  
5  
6  
7 CH<sub>2</sub>Cl<sub>2</sub>/petroleum ether (1/1) to give the final product.  
8  
9

10 *BF<sub>2</sub> Chelate of [4-bromo-5-(4-methoxyphenyl)-3-phenyl-1H-pyrrol-2-yl][5-(4-*  
11  
12  
13  
14 *methoxyphenyl)-3-phenylpyrrol-2-ylidene]amine (3)*, coppery solid, yield 93.5%. <sup>1</sup>H NMR  
15  
16  
17 (400 MHz, CDCl<sub>3</sub>) δ 8.10 – 8.00 (m, 4H), 7.89 (d, *J* = 7.0 Hz, 2H), 7.77 (d, *J* = 8.7 Hz,  
18  
19  
20 2H), 7.48 (dt, *J* = 13.7, 6.9 Hz, 3H), 7.41 – 7.35 (m, 3H), 7.11 (s, 1H), 7.02 (d, *J* = 8.8 Hz,  
21  
22  
23 2H), 6.96 (d, *J* = 8.9 Hz, 2H), 3.87 (s, 3H), 3.85 (s, 3H). <sup>13</sup>C NMR (151 MHz, CDCl<sub>3</sub>) δ  
24  
25  
26 162.26, 161.24, 160.44, 152.67, 146.29, 144.69, 141.90, 139.11, 131.76, 131.66, 131.62,  
27  
28  
29 131.01, 130.83, 130.21, 129.23, 128.64, 128.28, 127.99, 127.28, 122.55, 121.98, 119.11,  
30  
31  
32 113.86, 112.82, 107.67, 54.88, 54.64, 28.70. HRMS (DART) *m/z*: 635.1300 [M + H]<sup>+</sup>,  
33  
34  
35  
36  
37  
38 calcd for C<sub>34</sub>H<sub>26</sub>BBrF<sub>2</sub>N<sub>3</sub>O<sub>2</sub> 635.1300.  
39  
40

41 *BF<sub>2</sub> Chelate of [4-iodo-5-(4-methoxyphenyl)-3-phenyl-1H-pyrrol-2-yl][5-(4-*  
42  
43  
44  
45 *methoxyphenyl)-3-phenylpyrrol-2-ylidene]amine (4)*, coppery solid, yield 89.2%. <sup>1</sup>H NMR  
46  
47  
48 (400 MHz, CDCl<sub>3</sub>) δ 8.09 – 7.99 (m, 4H), 7.86 – 7.80 (m, 2H), 7.70 (d, *J* = 8.6 Hz, 2H),  
49  
50  
51 7.54 – 7.42 (m, 3H), 7.37 (dd, *J* = 5.2, 1.9 Hz, 3H), 7.12 (s, 1H), 7.04 – 6.99 (m, 2H), 6.98  
52  
53  
54 – 6.93 (m, 2H), 3.88 (s, 3H), 3.85 (s, 3H). <sup>13</sup>C NMR (151 MHz, CDCl<sub>3</sub>) δ 162.28, 161.28,  
55  
56  
57  
58  
59  
60

1  
2  
3 160.34, 155.70, 146.19, 144.80, 143.95, 142.83, 132.08, 131.81, 131.67, 131.63, 131.60,  
4  
5  
6  
7 130.99, 130.23, 129.23, 128.62, 128.25, 127.98, 127.17, 123.49, 122.53, 119.24, 113.87,  
8  
9  
10 112.69, 80.03, 54.87, 54.63, 29.07, 28.70. HRMS (DART)  $m/z$ : 683.1158 [M + H]<sup>+</sup>, calcd  
11  
12  
13  
14 for C<sub>34</sub>H<sub>26</sub>BF<sub>2</sub>IN<sub>3</sub>O<sub>2</sub> 683.1162.

15  
16  
17 *BF<sub>2</sub> Chelate of [4-bromo-3-phenyl-5-(4-tolyl)-1H-pyrrol-2-yl][3-phenyl-5-(4-tolyl)-pyrrol-*  
18  
19  
20  
21 *2-ylidene]amine (8)*, coppery solid, yield 90.4%. <sup>1</sup>H NMR (400 MHz, CDCl<sub>3</sub>) δ 8.05 (dd, *J*  
22  
23 = 6.7, 3.0 Hz, 2H), 7.93 (dd, *J* = 13.3, 7.6 Hz, 4H), 7.69 (d, *J* = 7.6 Hz, 2H), 7.49 (dd, *J* =  
24  
25 = 6.7, 3.0 Hz, 2H), 7.93 (dd, *J* = 13.3, 7.6 Hz, 4H), 7.69 (d, *J* = 7.6 Hz, 2H), 7.49 (dd, *J* =  
26  
27 12.2, 6.9 Hz, 3H), 7.44 – 7.36 (m, 3H), 7.34 – 7.23 (m, 4H), 7.10 (s, 1H), 2.44 (s, 3H),  
28  
29 2.40 (s, 3H). <sup>13</sup>C NMR (151 MHz, CDCl<sub>3</sub>) δ 161.94, 154.08, 146.19, 145.00, 142.23,  
30  
31 142.08, 139.90, 139.83, 131.02, 130.69, 130.22, 129.85, 129.30, 129.27, 128.96, 128.67,  
32  
33 128.45, 128.08, 128.02, 127.46, 127.32, 126.62, 119.19, 108.02, 29.08, 28.71, 21.08.  
34  
35  
36  
37  
38  
39  
40  
41  
42 HRMS (DART)  $m/z$ : 603.1395 [M + H]<sup>+</sup>, calcd for C<sub>34</sub>H<sub>26</sub>BBrF<sub>2</sub>N<sub>3</sub> 603.1402.

43  
44  
45 *BF<sub>2</sub> Chelate of [4-iodo-3-phenyl-5-(4-tolyl)-1H-pyrrol-2-yl][3-phenyl-5-(4-tolyl)-pyrrol-2-*  
46  
47  
48  
49 *ylidene]amine (9)*, coppery solid, yield 87.5%. <sup>1</sup>H NMR (400 MHz, CDCl<sub>3</sub>) δ 8.05 – 7.97  
50  
51 (m, 2H), 7.91 (d, *J* = 8.1 Hz, 2H), 7.86 – 7.80 (m, 2H), 7.60 (d, *J* = 7.9 Hz, 2H), 7.53 –  
52  
53 7.41 (m, 3H), 7.36 (dd, *J* = 5.3, 1.9 Hz, 3H), 7.28 (d, *J* = 7.9 Hz, 2H), 7.24 (d, *J* = 4.9 Hz,  
54  
55  
56  
57  
58  
59  
60

1  
2  
3  
4 2H), 7.08 (s, 1H), 2.42 (s, 3H), 2.37 (s, 3H).  $^{13}\text{C}$  NMR (151 MHz,  $\text{CDCl}_3$ )  $\delta$  161.89, 157.13,  
5  
6  
7 146.04, 145.06, 144.75, 143.17, 142.07, 139.73, 131.91, 131.01, 130.23, 129.90, 129.28,  
8  
9  
10 129.25, 128.96, 128.65, 128.41, 128.14, 128.01, 127.99, 127.47, 127.21, 119.29, 80.37,  
11  
12  
13  
14 21.08. HRMS (DART)  $m/z$ : 651.1259  $[\text{M} + \text{H}]^+$ , calcd for  $\text{C}_{34}\text{H}_{26}\text{BF}_2\text{IN}_3$  651.1263.

15  
16  
17 *BF<sub>2</sub> Chelate of [4-iodo-5-(5-methylthiophen-2-yl)-3-phenyl-1H-pyrrol-2-yl][5-(5-*  
18  
19  
20  
21 *methylthiophen-2-yl)-3-phenylpyrrol-2-ylidene]amine (11)*, coppery solid, yield 83.1%.  $^1\text{H}$   
22  
23  
24 NMR (400 MHz,  $\text{CDCl}_3$ )  $\delta$  8.22 (d,  $J$  = 4.0 Hz, 1H), 8.04 – 7.98 (m, 2H), 7.78 (dt,  $J$  = 6.1,  
25  
26  
27 1.5 Hz, 2H), 7.73 (d,  $J$  = 3.7 Hz, 1H), 7.53 – 7.42 (m, 3H), 7.37 (dt,  $J$  = 5.6, 3.3 Hz, 3H),  
28  
29  
30  
31 7.18 (s, 1H), 6.97 – 6.91 (m, 2H), 2.62 (s, 3H), 2.60 (s, 3H).  $^{13}\text{C}$  NMR (151 MHz,  $\text{CDCl}_3$ )  
32  
33  
34  $\delta$  153.42, 151.56, 147.90, 147.15, 145.71, 144.75, 144.05, 143.51, 136.58, 133.88,  
35  
36  
37  
38 132.91, 131.29, 131.12, 130.96, 129.90, 129.81, 129.57, 129.14, 128.70, 128.59, 127.70,  
39  
40  
41  
42 126.17, 119.92, 16.15, 15.66. HRMS (DART)  $m/z$ : 663.0384  $[\text{M} + \text{H}]^+$ , calcd for  
43  
44  
45  $\text{C}_{30}\text{H}_{22}\text{BF}_2\text{IN}_3\text{S}_2$  663.0392.

46  
47  
48  
49 *BF<sub>2</sub> Chelate of [4-bromo-5-(4-methoxyphenyl)-3-phenyl-1H-pyrrol-2-yl][4,5-Dihydro-7-*  
50  
51  
52 *methoxy-3-phenylethylbenzo[g]indole-2-ylidene]amine (12)*, coppery solid, yield 87.4%.  
53  
54  
55  
56  $^1\text{H}$  NMR (400 MHz,  $\text{CDCl}_3$ )  $\delta$  8.61 (d,  $J$  = 9.1 Hz, 1H), 7.87 (dt,  $J$  = 6.4, 1.4 Hz, 2H), 7.81  
57  
58  
59  
60

1  
2  
3  
4 – 7.72 (m, 2H), 7.72 – 7.64 (m, 2H), 7.49 – 7.34 (m, 6H), 7.07 – 7.00 (m, 2H), 6.90 (dd,  $J$   
5  
6 = 9.0, 2.7 Hz, 1H), 6.81 (d,  $J$  = 2.6 Hz, 1H), 3.89 (s, 3H), 3.87 (s, 3H), 2.94 (m, 4H).  $^{13}\text{C}$   
7  
8  
9  
10 NMR (151 MHz,  $\text{CDCl}_3$ )  $\delta$  163.17, 159.95, 158.06, 149.07, 147.34, 145.41, 140.95,  
11  
12  
13  
14 139.21, 136.42, 133.16, 132.65, 131.75, 131.20, 130.58, 130.06, 129.67, 128.30, 127.72,  
15  
16  
17 127.58, 127.14, 122.60, 118.56, 114.02, 112.97, 112.71, 105.93, 54.97, 54.61, 29.73,  
18  
19  
20  
21 21.37. HRMS (DART)  $m/z$ : 661.1451  $[\text{M} + \text{H}]^+$ , calcd for  $\text{C}_{36}\text{H}_{28}\text{BBrF}_2\text{N}_3\text{O}_2$  661.1457.

22  
23  
24 *BF<sub>2</sub> Chelate of [4-bromo-5-(4-tolyl)-3-phenyl-1H-pyrrol-2-yl][4,5-Dihydro-7-methoxy-3-*  
25  
26  
27  
28 *phenylethylbenzo[g]indole-2-ylidene]amine (13)*, coppery solid, yield 93.6%.  $^1\text{H}$  NMR  
29  
30  
31 (400 MHz,  $\text{CDCl}_3$ )  $\delta$  8.61 (d,  $J$  = 9.1 Hz, 1H), 7.87 (dt,  $J$  = 6.6, 1.4 Hz, 2H), 7.71 – 7.64  
32  
33  
34 (m, 4H), 7.47 – 7.35 (m, 6H), 7.32 (d,  $J$  = 7.9 Hz, 2H), 6.89 (dd,  $J$  = 9.0, 2.7 Hz, 1H), 6.81  
35  
36  
37 (d,  $J$  = 2.6 Hz, 1H), 3.87 (s, 3H), 2.94 (dt,  $J$  = 7.4, 3.2 Hz, 4H), 2.45 (s, 3H).  $^{13}\text{C}$  NMR (151  
38  
39  
40  
41 MHz,  $\text{CDCl}_3$ )  $\delta$  163.27, 158.49, 149.03, 147.49, 145.51, 140.81, 139.39, 138.91, 136.17,  
42  
43  
44  
45 133.32, 132.90, 132.83, 132.75, 131.22, 130.53, 130.04, 129.67, 128.34, 127.98, 127.69,  
46  
47  
48 127.59, 127.45, 127.14, 118.48, 114.03, 113.01, 105.70, 54.97, 29.71, 21.39, 21.06.  
49  
50  
51  
52 HRMS (DART)  $m/z$ : 645.1501  $[\text{M} + \text{H}]^+$ , calcd for  $\text{C}_{36}\text{H}_{28}\text{BBrF}_2\text{N}_3\text{O}$  645.1508.  
53  
54  
55  
56  
57  
58  
59  
60

1  
2  
3  
4 *BF<sub>2</sub> Chelate of [4-bromo-5-(5-methylthiophen-2-yl)-3-phenyl-1H-pyrrol-2-yl][4,5-*  
5  
6  
7 *Dihydro-7-methoxy-3-phenylethylbenzo[g]indole-2-ylidene]amine (14)*, coppery solid,  
8  
9  
10  
11 yield 89.4%. <sup>1</sup>H NMR (400 MHz, CDCl<sub>3</sub>) δ 8.74 (d, *J* = 9.2 Hz, 1H), 7.85 – 7.78 (m, 3H),  
12  
13  
14 7.71 – 7.65 (m, 2H), 7.48 – 7.35 (m, 6H), 6.98 (dd, *J* = 9.2, 2.7 Hz, 1H), 6.92 (d, *J* = 3.7  
15  
16  
17 Hz, 1H), 6.84 (d, *J* = 2.6 Hz, 1H), 3.91 (q, *J* = 2.1, 1.4 Hz, 3H), 2.96 (s, 4H), 2.61 (s, 3H).  
18  
19  
20  
21 <sup>13</sup>C NMR (151 MHz, CDCl<sub>3</sub>) δ 163.74, 158.29, 148.11, 146.05, 145.30, 142.75, 141.90,  
22  
23  
24 139.46, 137.69, 133.83, 133.34, 133.20, 131.65, 131.18, 130.78, 130.26, 128.89, 128.41,  
25  
26  
27 128.20, 127.72, 126.18, 119.31, 114.66, 113.67, 55.63, 30.39, 22.01, 15.61. HRMS  
28  
29  
30  
31 (DART) *m/z*. 651.1063 [M + H]<sup>+</sup>, calcd for C<sub>34</sub>H<sub>26</sub>BBrF<sub>2</sub>N<sub>3</sub>OS 651.1072.  
32  
33

34  
35 *BF<sub>2</sub> Chelate of [4-iodo-5-(4-methoxyphenyl)-3-phenyl-1H-pyrrol-2-yl][4,5-Dihydro-7-*  
36  
37  
38 *methoxy-3-phenylethylbenzo[g]indole-2-ylidene]amine (15)*, coppery solid, yield 85.4%.  
39  
40  
41  
42 <sup>1</sup>H NMR (400 MHz, CDCl<sub>3</sub>) δ 8.61 (d, *J* = 9.0 Hz, 1H), 7.86 – 7.78 (m, 2H), 7.75 – 7.63  
43  
44  
45 (m, 4H), 7.53 – 7.34 (m, 6H), 7.09 – 7.01 (m, 2H), 6.91 (dd, *J* = 9.0, 2.6 Hz, 1H), 6.82 (d,  
46  
47  
48 *J* = 2.6 Hz, 1H), 3.91 (s, 3H), 3.88 (s, 3H), 2.94 (q, *J* = 4.4, 3.8 Hz, 4H). <sup>13</sup>C NMR (151  
49  
50  
51 MHz, CDCl<sub>3</sub>) δ 163.18, 159.89, 158.06, 152.32, 147.20, 145.41, 141.87, 141.02, 139.27,  
52  
53  
54  
55 133.29, 132.68, 132.38, 131.85, 130.57, 130.13, 129.65, 128.28, 127.71, 127.57, 127.03,  
56  
57  
58  
59  
60

1  
2  
3  
4 124.14, 118.54, 114.02, 112.97, 112.59, 78.08, 54.96, 54.60, 29.72, 21.41. HRMS  
5  
6  
7 (DART)  $m/z$ . 709.1309 [M + H]<sup>+</sup>, calcd for C<sub>36</sub>H<sub>28</sub>BF<sub>2</sub>IN<sub>3</sub>O<sub>2</sub> 709.1318.  
8  
9

10 *BF<sub>2</sub> Chelate of [4-iodo-5-(4-tolyl)-3-phenyl-1H-pyrrol-2-yl][4,5-Dihydro-7-methoxy-3-*  
11 *phenylethylbenzo[g]indole-2-ylidene]amine (16)*, coppery solid, yield 89.0%. <sup>1</sup>H NMR  
12  
13  
14  
15  
16  
17 (400 MHz, CDCl<sub>3</sub>) δ 8.59 (d,  $J$  = 9.1 Hz, 1H), 7.84 – 7.78 (m, 2H), 7.68 – 7.63 (m, 2H),  
18  
19  
20  
21 7.61 (d,  $J$  = 7.9 Hz, 2H), 7.47 – 7.35 (m, 6H), 7.32 (d,  $J$  = 7.9 Hz, 2H), 6.88 (dd,  $J$  = 9.0,  
22  
23  
24 2.7 Hz, 1H), 6.80 (d,  $J$  = 2.6 Hz, 1H), 3.86 (s, 3H), 2.94 (td,  $J$  = 7.4, 4.7 Hz, 4H), 2.46 (s,  
25  
26  
27 3H). <sup>13</sup>C NMR (151 MHz, CDCl<sub>3</sub>) δ 163.27, 158.42, 152.35, 147.33, 145.49, 141.73,  
28  
29  
30  
31 140.75, 139.41, 138.82, 133.42, 132.84, 132.76, 132.38, 130.53, 130.13, 129.66, 129.00,  
32  
33  
34  
35 128.32, 127.89, 127.68, 127.58, 127.03, 118.48, 114.02, 113.01, 77.75, 54.97, 29.71,  
36  
37  
38 28.70, 21.42, 21.08. HRMS (DART)  $m/z$ . 693.1356 [M + H]<sup>+</sup>, calcd for C<sub>36</sub>H<sub>28</sub>BF<sub>2</sub>IN<sub>3</sub>O  
39  
40  
41 693.1369.  
42  
43  
44

45 *BF<sub>2</sub> Chelate of [4-iodo-5-(5-methylthiophen-2-yl)-3-phenyl-1H-pyrrol-2-yl][4,5-Dihydro-*  
46 *7-methoxy-3-phenylethylbenzo[g]indole-2-ylidene]amine (17)*, coppery solid, yield  
47  
48  
49 87.2%. <sup>1</sup>H NMR (400 MHz, CDCl<sub>3</sub>) δ 8.71 (d,  $J$  = 9.1 Hz, 1H), 7.79 – 7.73 (m, 2H), 7.68 –  
50  
51  
52 7.63 (m, 2H), 7.59 (d,  $J$  = 3.7 Hz, 1H), 7.47 – 7.36 (m, 6H), 6.96 (dd,  $J$  = 9.0, 2.7 Hz, 1H),  
53  
54  
55  
56  
57  
58  
59  
60

1  
2  
3  
4 6.90 (dd,  $J = 3.7, 1.1$  Hz, 1H), 6.83 (d,  $J = 2.6$  Hz, 1H), 3.90 (s, 3H), 2.97 – 2.93 (m, 4H),

5  
6  
7 2.61 (d,  $J = 1.1$  Hz, 3H).  $^{13}\text{C}$  NMR (151 MHz,  $\text{CDCl}_3$ )  $\delta$  163.92, 158.80, 148.17, 146.18,

8  
9  
10 145.85, 144.54, 142.63, 142.16, 139.75, 134.11, 133.48, 133.05, 131.14, 130.85, 130.27,

11  
12  
13 130.07, 129.89, 128.93, 128.35, 128.20, 127.62, 125.88, 55.63, 30.37, 22.07, 15.61.

14  
15  
16  
17 HRMS (DART)  $m/z$ : 699.0923  $[\text{M} + \text{H}]^+$ , calcd for  $\text{C}_{34}\text{H}_{26}\text{BF}_2\text{IN}_3\text{OS}$  699.0933.

18  
19  
20  
21 *BF<sub>2</sub> Chelate of [4-iodo-5-(thiophen-2-yl)-3-phenyl-1H-pyrrol-2-yl][4,5-Dihydro-7-*  
22  
23  
24 *methoxy-3-phenylethylbenzo[g]indole-2-ylidene]amine (18)*, coppery solid, yield 83.4%.

25  
26  
27  
28  $^1\text{H}$  NMR (400 MHz,  $\text{CDCl}_3$ )  $\delta$  8.70 (d,  $J = 9.1$  Hz, 1H), 7.78 (dt,  $J = 6.4, 1.4$  Hz, 2H), 7.71

29  
30  
31 (dd,  $J = 3.8, 1.2$  Hz, 1H), 7.66 (dd,  $J = 7.6, 2.1$  Hz, 2H), 7.61 (dd,  $J = 5.1, 1.2$  Hz, 1H),

32  
33  
34 7.48 – 7.36 (m, 6H), 7.23 (dd,  $J = 5.1, 3.7$  Hz, 1H), 6.95 (dd,  $J = 9.0, 2.7$  Hz, 1H), 6.83 (d,

35  
36  
37  $J = 2.6$  Hz, 1H), 3.90 (s, 3H), 2.96 (td,  $J = 6.8, 4.5$  Hz, 4H).  $^{13}\text{C}$  NMR (151 MHz,  $\text{CDCl}_3$ )

38  
39  
40  $\delta$  164.21, 159.72, 148.52, 146.49, 144.95, 142.36, 141.43, 140.12, 134.50, 133.74,

41  
42  
43 133.00, 132.54, 132.38, 131.00, 130.82, 130.28, 129.05, 128.99, 128.33, 128.23, 127.64,

44  
45  
46  
47 127.05, 119.02, 114.73, 113.79, 55.66, 30.33, 22.09. HRMS (DART)  $m/z$ : 685.0771  $[\text{M} +$

48  
49  
50  
51  
52  $\text{H}]^+$ , calcd for  $\text{C}_{33}\text{H}_{24}\text{BF}_2\text{IN}_3\text{OS}$  685.0777.

1  
2  
3  
4 *Synthetic procedure for mixed halogenated aza-BODIPY photosensitizers BF<sub>2</sub> Chelate*  
5  
6  
7 *of [4-bromo-5-(4-methoxyphenyl)-3-phenyl-1H-pyrrol-2-yl][4-iodo-5-(4-methoxyphenyl)-*  
8  
9  
10 *3-phenylpyrrol-2-ylidene]amine (5):*

11  
12  
13  
14 **4** (0.036 mmol) was dissolved in CH<sub>2</sub>Cl<sub>2</sub> (6 ml), acetic acid (2 ml) was added, followed  
15  
16  
17 by the addition of NBS (0.036 mmol) and allowed to react at room temperature for 30 min.

18  
19  
20  
21 The mixture were washed with sodium sulfate aqueous and CH<sub>2</sub>Cl<sub>2</sub> for three times, and  
22  
23  
24 the organic phases were combined and separated by column chromatography with

25  
26  
27  
28 CH<sub>2</sub>Cl<sub>2</sub> as eluent. The product was recrystallized from CH<sub>2</sub>Cl<sub>2</sub>/petroleum ether (1/1) to  
29  
30  
31 give the final product (coppery solid, yield 88.7%). <sup>1</sup>H NMR (400 MHz, CDCl<sub>3</sub>) δ 7.89 –

32  
33  
34  
35 7.67 (m, 8H), 7.47 – 7.41 (m, 6H), 7.02 – 6.97 (m, 4H), 3.89 – 3.85 (m, 6H). <sup>13</sup>C NMR (151  
36  
37  
38 MHz, CDCl<sub>3</sub>) δ 161.72, 161.55, 160.31, 157.62, 147.71, 145.08, 144.07, 142.66, 132.43,

39  
40  
41  
42 131.94, 130.74, 129.46, 129.41, 127.96, 127.87, 123.26, 121.76, 113.59, 113.44, 55.32,  
43  
44  
45 55.30, 53.43. HRMS (DART) *m/z*. 761.0268 [M + H]<sup>+</sup>, calcd for C<sub>34</sub>H<sub>25</sub>BBrF<sub>2</sub>IN<sub>3</sub>O<sub>2</sub>

46  
47  
48  
49 761.0267.

#### 50 51 52 **4.2 Absorption and emission spectra.**

53  
54  
55  
56  
57  
58  
59  
60

1  
2  
3 The absorption and emission spectra of **4** in various reagent were recorded on a 759S  
4  
5  
6  
7 UV-visible spectrophotometer (Lengguang Tech, China) and F98 fluorescence  
8  
9  
10 spectrophotometer (Lengguang Tech, China). All the measurements were carried out at  
11  
12  
13  
14 room temperature.  
15  
16

### 17 4.3. Fluorescence quantum yield.

18  
19  
20  
21 Fluorescence quantum yields ( $\Phi_f$ ) were measured as reported and calculated by the  
22  
23  
24 equation:  $\Phi_{f(s)} = (F_s/F_{ref}) \cdot (n_s^2/n_{ref}^2) \cdot (A_{ref}/A_s) \cdot \Phi_{f(ref)}$ ,<sup>52</sup> wherein F, A and n represent the  
25  
26  
27 area under the emission peak of measured fluorescence, the absorbance at the excitation  
28  
29  
30 position (670 nm), and the refractive index of the solvent, respectively. Compound **A** was  
31  
32  
33 used as the reference in  $\text{CHCl}_3$  ( $\Phi_f = 0.36$ ). The emission spectra were obtained in very  
34  
35  
36 dilute solutions ( $\text{Abs} \leq 0.010$ ) to minimize reabsorption effect of radiation.  
37  
38  
39  
40

### 41 4.4 Singlet oxygen quantum yield.

42  
43  
44  
45 The singlet oxygen quantum yields ( $\Phi_\Delta$ ) were determined as reported by using DPBF  
46  
47  
48 as the singlet oxygen scavenger and ZnPc as the reference ( $\Phi_\Delta = 0.56$  in DMF).<sup>66</sup> The  
49  
50  
51 light source is composed of a 75 W halogen lamp, a 590 nm cutoff optical filter (Sipeida,  
52  
53  
54  
55 China) and a water tank for cooling. A solution of DPBF (50  $\mu\text{M}$ ) containing the  
56  
57  
58  
59  
60

1  
2  
3 photosensitizer (1  $\mu\text{M}$ ) in DMF was prepared in the dark and then irradiated with filtered  
4  
5  
6  
7 red light ( $\lambda > 590 \text{ nm}$ ). The maximum absorption values (411 nm) of DPBF was monitored  
8  
9  
10 along with irradiated time. The  $\Phi_{\Delta}$  values were determined according to the equation  $\Phi_{\Delta(s)}$   
11  
12  
13  $= (K_s/K_{\text{ref}}) \cdot (A_{\text{ref}}/A_s) \cdot \Phi_{\Delta(\text{ref})}$ , where  $\Phi_{\Delta(\text{ref})}$  is the singlet oxygen quantum yield of reference  
14  
15  
16  
17 ZnPc in DMF,  $K_s$  and  $K_{\text{ref}}$  are the photobleaching rates of DPBF in the presence of the  
18  
19  
20 samples and ZnPc,  $A_s$  and  $A_{\text{ref}}$  represent the absorption areas of Q band (590–750 nm)  
21  
22  
23  
24 of the samples and ZnPc respectively. As for the relative rate of DPBF degradation,  
25  
26  
27  
28 methylene blue (1  $\mu\text{M}$ ) was used as reference in  $\text{tPrOH}$  and emulsified PBS system.  
29  
30

#### 31 **4.5. Cell lines and culture conditions.**

32  
33  
34  
35 Human cervical cancer cell line HeLa, human breast cancer cell line MCF-7 and human  
36  
37  
38 colon cell line SW480 were obtained from American Type Culture Collection (ATCC). All  
39  
40  
41  
42 cells were cultured in Dulbecco's modified Eagle's medium (GE Healthcare Life Sciences,  
43  
44  
45 USA), supplemented with 10% fetal bovine serum and 1% penicillin–streptomycin (GE  
46  
47  
48  
49 Healthcare Life Sciences, USA) in a humidified incubator at 37 °C with an atmosphere of  
50  
51  
52 5%  $\text{CO}_2$ .  
53  
54  
55

#### 56 **4.6. Cytotoxicity study.**

1  
2  
3  
4 The phototoxicity of photosensitizers were determined in human cervical cancer cells  
5  
6  
7 following the procedures as reported. Briefly, the photosensitizer ( $6.0 \times 10^{-6}$  mol) was  
8  
9  
10 dissolved in THF (2.0 ml) and a mixture of Cremophor EL (CrEL)/1,2-propanediol (10:3,  
11  
12  
13 v:v) (0.1 ml) was added, then the solution was placed in a sonic bath for 10 min. THF was  
14  
15  
16 removed under reduced pressure, then the mixture was dissolved in phosphate-buffered  
17  
18  
19 saline (PBS) (7 ml). The solution was then passed through a filter membrane (13 mm  $\times$   
20  
21  
22 0.22  $\mu$ m, Tansoole, China). The exact concentration of the photosensitizer was confirmed  
23  
24  
25 by UV – Visible spectral when used for assaying.  $3 \times 10^3$  cells/well were seeded on a 96-  
26  
27  
28 well culture plates (Corning Inc., USA) and allowed to adhere overnight. The cells were  
29  
30  
31 incubated with various photosensitizers of different concentrations for 3 h and then  
32  
33  
34 irradiated with a light dose of 54 J/cm<sup>2</sup> ( $\lambda > 590$  nm), followed by incubation for 24 h in a  
35  
36  
37 humidified incubator at 37 °C. After treatment, the above loading media was removed and  
38  
39  
40 then 100  $\mu$ L of MTT solution (0.5 mg/mL in PBS) was added to each well, which was then  
41  
42  
43 incubated for 4 h at 37 °C in a humidified incubator. Subsequently, the MTT-containing  
44  
45  
46 medium was removed and DMSO was added (100  $\mu$ L per well) to dissolve the formazan  
47  
48  
49 crystals. The absorbance at 490 nm was measured using a SpectraMax M5 microplate  
50  
51  
52  
53  
54  
55  
56  
57  
58  
59  
60

1  
2  
3 reader (Molecular Devices, USA). For dark toxicity, no light dose was provided and cell  
4  
5  
6  
7 viability was measured as described above.  
8  
9

#### 10 **4.7 Apoptosis assay.**

11  
12 Apoptosis assay were conducted using annexin V-FITC/PI (Beyotime Biotechnology,  
13  
14 China) double staining following the manufacturer's protocol. Briefly, HeLa cells were  
15  
16  
17 seeded in six-well plate and incubated with **4** for 3 h and then irradiated with a light dose  
18  
19  
20  
21 of 54 J/cm<sup>2</sup> ( $\lambda > 590$  nm), followed by incubation for 24 h in a humidified incubator at 37  
22  
23  
24  
25 °C. After treatment, the above loading media was removed and cells were harvested  
26  
27  
28  
29 respectively, then washed with PBS and stained with a mixture of annexin V(2  $\mu$ L) and PI  
30  
31  
32 (2  $\mu$ L) followed by incubation for 20 min at room temperature. Apoptosis was then  
33  
34  
35  
36  
37  
38 determined immediately using flow cytometry (Beckman, USA).  
39  
40

#### 41 **4.8 Subcellular localization.**

42  
43 HeLa cells were seeded on 35 mm diameter glass-bottom culture dish (NEST,  
44  
45  
46 Cat.No.801001) and allowed to adhere overnight in a humidified incubator at 37 °C under  
47  
48  
49  
50  
51  
52 5% CO<sub>2</sub> atmosphere. The medium was replaced with fresh medium containing 5  $\mu$ M  
53  
54  
55  
56 photosensitizer **4** and incubated in dark for 2 h. The medium was then removed, washed  
57  
58  
59  
60

1  
2  
3 twice with PBS, followed by incubation with Mito-Tracker Green FM (250 nM, 30 min,  
4  
5  
6  
7 Molecular Probes, Yeasen, China), ER-Tracker Green (2  $\mu$ M, 45 min, Molecular Probes,  
8  
9  
10 Yeasen, China) and Lyso-Tracker Green DND-26 (160 nM, 30 min, Molecular Probes,  
11  
12  
13 Life Technologies, USA) in a humidified incubator at 37 °C with an atmosphere of 5%  
14  
15  
16  
17 CO<sub>2</sub>. Then the trackers-containing medium were removed and washed twice with PBS,  
18  
19  
20  
21 the cells were re-fed with fresh DMEM and imaged on a confocal scanning microscope  
22  
23  
24 (Carl Zeiss LSM 710) equipped with a 488 nm argon laser and a 633 nm laser. The  
25  
26  
27  
28 excitation wavelength of all Trackers was 488 nm and their fluorescence was collected at  
29  
30  
31 500–560 nm, while **4** was excited at 633 nm and its fluorescence was monitored at  
32  
33  
34  
35 650–740 nm.

#### 38 **4.9 Investigation of intracellular ROS level.**

39  
40  
41  
42 HeLa cells were incubated with solutions of **4** with variant concentrations (0.004, 0.02,  
43  
44  
45 0.10, 0.5, 2.5  $\mu$ M) for 3 h on 35 mm diameter glass-bottom culture dish (Nest, Cat. No.  
46  
47  
48 801001) or 96-well plates (Corning Inc., costar, 3603). The cells were then washed twice  
49  
50  
51  
52 with PBS and incubated with H<sub>2</sub>DCFDA (Molecular Probes, Life Technologies, D399) in  
53  
54  
55  
56 PBS (10  $\mu$ M, 100  $\mu$ L) for 20 min at 37 °C in the incubator. After being washed twice with  
57  
58  
59  
60

1  
2  
3  
4 PBS, the cells were re-fed with PBS and irradiated with a light dose of 54 J/cm<sup>2</sup> ( $\lambda > 590$   
5  
6  
7 nm). The cells were then imaged on a confocal scanning microscope (Carl Zeiss LSM  
8  
9  
10 710). Meanwhile, the fluorescence signal was measured by a SpectraMax M5 microplate  
11  
12  
13 reader (Molecular Devices, USA) using a 485 nm excitation filter and a 538 nm emission  
14  
15  
16  
17 filter.  
18

#### 21 **4.10. Animals.**

22  
23  
24 Female Balb C nu/nu mice were purchased from Shanghai Slac Laboratory Animal Co.  
25  
26  
27 Ltd. (Shanghai, China). HeLa tumor cells were injected subcutaneously into the right back  
28  
29  
30 of nude mice and the cell density was about  $5 \times 10^6$  per mouse. On the seventh day after  
31  
32  
33 inoculation, nude mice with a body weight of 18–22 g and a tumor volume of 80–100 mm<sup>3</sup>  
34  
35  
36 were subjected to PDT and started to count as day zero. The animal experimental  
37  
38  
39 procedures were carried out according to the Guidelines of the Animal Ethical Care and  
40  
41  
42 Use Committee, Fudan University.  
43  
44  
45

#### 49 **4.11 *In vivo* and *ex vivo* imaging.**

50  
51  
52 The mice were injected with **4** (2 mg/kg) via the tail vein and imaged using a VISQUE  
53  
54  
55 Invivo Smart imaging system (Vieworks Co., Ltd., Korean) with excitation of 680 nm and  
56  
57  
58

1  
2  
3 emission of 720 nm. The living mice were then anesthetized with isoflurane and imaged  
4  
5  
6  
7 at various time points after 15 min of tail vein injection. To investigate the organ  
8  
9  
10 biodistribution of **4**, the mice was then euthanized, major normal organs (heart, liver,  
11  
12  
13 spleen, lungs, kidneys) as well as tumors were extracted, which were placed on black  
14  
15  
16 paper and *ex vivo* fluorescence images were obtained. Images were analyzed using  
17  
18  
19 VISQUE Invivo Smart analysis system. Regions of interest (ROI) were drawn over the  
20  
21  
22 tumor and major organs to acquire the quantitative comparison. All results were obtained  
23  
24  
25 as the mean  $\pm$  standard deviation (SD) for a group of three mice. All fluorescence images  
26  
27  
28 were acquired using a 1 s exposure time (f/stop = 4), with animal remaining sedated to  
29  
30  
31 obtain multiple angles samples.  
32  
33  
34  
35  
36  
37

#### 38 **4.12 PDT effects on HeLa xenograft model.**

39  
40  
41 **ADPM06** and the commercially available photosensitizer **Ce6** were used as references  
42  
43  
44 to compare the anti-tumor effects of **4**. Nude mice were randomly divided into four groups,  
45  
46  
47 including control group, **ADPM06** group, **4** group and **Ce6** group, each group contained  
48  
49  
50 five mice. The control group was given the same amount of saline. The experimental  
51  
52  
53 group was injected with the photosensitizer (2 mg/kg) via tail vein injection. After 15 min  
54  
55  
56  
57  
58  
59  
60

1  
2  
3 of injection, the tumor site was irradiated with light. The light source contains a 75 W  
4  
5  
6 halogen lamp, a color filter with cut-on at 590 nm (Sipeida, China) and a water tank for  
7  
8  
9  
10 cooling. The irradiation time of each nude mouse was 10 min and the light dose was 54  
11  
12  
13 J/cm<sup>2</sup>. After treatment, the long (L) and short diameter (W) of tumors were recorded using  
14  
15  
16  
17 a digital vernier caliper every other day, and the body weight was measured as well.  
18  
19  
20  
21 Tumor volume was calculated using the formula:  $V = 0.5 \times (L \times W^2)$ .  
22  
23

#### 24 **4.13 Statistical analysis.**

25  
26  
27 Comparisons among the groups were analyzed using t tests one-way ANOVA followed  
28  
29  
30  
31 by Tukey's multiple comparison tests. Results were considered statistically significant at  
32  
33  
34  
35 a value of  $P < 0.05$ .  
36  
37

## 38 **ASSOCIATED CONTENT**

### 39 **Supporting Information**

40  
41  
42 The Supporting Information is available free of charge at  
43  
44  
45  
46  
47  
48  
49 <https://pubs.acs.org/doi/XX.XXXX/acs.jmedchem.XXXXXXX>.  
50

51  
52 Additional spectroscopic data and absorption spectra, figures of photodegradation of DPBF,  
53  
54 light dose-dependent cell viability, thermal stability of PSs, imaging of ROS generation in cells  
55  
56  
57  
58  
59  
60

1  
2  
3 and organ distributions in mice, copies of  $^1\text{H}$  and  $^{13}\text{C}$  NMR spectra, HRMS spectra (DART)  
4  
5  
6  
7 and HPLC spectra (PDF).  
8  
9

10 Molecular formula strings and the associated data (CSV).  
11  
12

## 13 14 **AUTHOR INFORMATION**

### 15 16 17 **Corresponding Author**

18  
19  
20  
21 \*For W.Z.: E-mail, zhaoweili@fudan.edu.cn; phone, +86 21 51980111.  
22  
23

24  
25 \*For X.D.: E-mail, xcdong@fudan.edu.cn; phone, +86 21 51980123.  
26  
27  
28

### 29 30 **Author Contributions**

31  
32  
33 #These authors contributed equally to this work. The manuscript was written through  
34  
35  
36 contributions of all authors. All authors have approved the final version of the manuscript.  
37  
38  
39

### 40 41 **Notes**

42  
43 The authors declare no competing financial interest.  
44  
45  
46

## 47 48 **ACKNOWLEDGMENT**

49  
50  
51 This research was supported by National Natural Science Foundation of China (No.  
52  
53  
54 21372063).  
55  
56  
57

## ABBREVIATIONS LIST

PDT, photodynamic therapy; PS, photosensitizer; BODIPY, 4,4-Difluoro-4-bora-3a,4a-diaza-s-indacene; NIR, near infrared; NBS, *N*-bromosuccinimide; NIS, *N*-iodosuccinimide; DMF, *N,N*-dimethylformamide; DMSO, dimethylsulfoxide; THF, tetrahydrofuran; TFA, trifluoroacetic acid; PBS, phosphate buffered saline; PI, propidium iodide; FBS, fetal bovine serum; DMEM, Dulbecco's Modified Eagle's Medium; MTT, 3-(4,5-dimethylthiazol-2-yl)-2,5-diphenyltetrazolium bromide; DPBF, 1,3-diphenylisobenzofuran; ROS, reactive oxygen species; H<sub>2</sub>DCFDA, 2',7'-dichlorodihydrofluorescein diacetate;  $\Phi_{\Delta}$ , singlet oxygen quantum yields;  $\Phi_f$ , fluorescence quantum yields.

## REFERENCES

- (1) Agostinis, P.; Berg, K.; Cengel, K. A.; Foster, T. H.; Girotti, A. W.; Gollnick, S. O.; Hahn, S. M.; Hamblin, M. R.; Juzeniene, A.; Kessel, D.; Korbelik, M.; Moan, J.; Mroz, P.; Nowis, D.; Piette, J.; Wilson, B. C.; Golab, J. Photodynamic therapy of cancer: an update. *Ca-Cancer J. Clin.* **2011**, *61*, 250-281.

1  
2  
3  
4 (2) Dolmans, D. E.; Fukumura, D.; Jain, R. K. Photodynamic therapy for cancer. *Nat.*  
5  
6  
7 *Rev. Cancer* **2003**, *3*, 380-387.

8  
9  
10  
11 (3) Castano, A. P.; Mroz, P.; Hamblin, M. R. Photodynamic therapy and anti-tumour  
12  
13  
14 immunity. *Nat. Rev. Cancer* **2006**, *6*, 535-545.

15  
16  
17  
18 (4) Celli, J. P.; Spring, B. Q.; Rizvi, I.; Evans, C. L.; Samkoe, K. S.; Verma, S.; Pogue,  
19  
20 B. W.; Hasan, T. Imaging and photodynamic therapy: mechanisms, monitoring, and  
21  
22  
23 optimization. *Chem. Rev.* **2010**, *110*, 2795-2838.

24  
25  
26  
27 (5) Lucky, S. S.; Soo, K. C.; Zhang, Y. Nanoparticles in photodynamic therapy. *Chem.*  
28  
29  
30 *Rev.* **2015**, *115*, 1990-2042.

31  
32  
33  
34 (6) Fernandes, S. R. G.; Fernandes, R.; Sarmiento, B.; Pereira, P. M. R.; Tome, J. P.  
35  
36  
37  
38 C. Photoimmunoconjugates: novel synthetic strategies to target and treat cancer by  
39  
40  
41  
42 photodynamic therapy. *Org. Biomol. Chem.* **2019**, *17*, 2579-2593.  
43  
44  
45  
46  
47  
48  
49  
50  
51  
52  
53  
54  
55  
56  
57  
58  
59  
60

1  
2  
3  
4 (7) Dai, Y.; Xu, C.; Sun, X.; Chen, X. Nanoparticle design strategies for enhanced  
5  
6  
7 anticancer therapy by exploiting the tumour microenvironment. *Chem. Soc. Rev.* **2017**,  
8  
9  
10 *46*, 3830-3852.

11  
12  
13  
14 (8) Lovell, J. F.; Liu, T. W.; Chen, J.; Zheng, G. Activatable photosensitizers for imaging  
15  
16  
17 and therapy. *Chem. Rev.* **2010**, *110*, 2839-2857.

18  
19  
20  
21 (9) Tang, Z.; Liu, Y.; He, M.; Bu, W. Chemodynamic therapy: tumour microenvironment-  
22  
23  
24 mediated fenton and fenton-like reactions. *Angew. Chem. Int. Ed.* **2019**, *58*, 946-956.

25  
26  
27 (10) Schweitzer, V. G. PHOTOFRIN-mediated photodynamic therapy for treatment of  
28  
29  
30 early stage oral cavity and laryngeal malignancies. *Lasers Surg. Med.* **2001**, *29*, 305-313.

31  
32  
33 (11) Yano, S.; Hirohara, S.; Obata, M.; Hagiya, Y.; Ogura, S.-i.; Ikeda, A.; Kataoka, H.;  
34  
35  
36 Tanaka, M.; Joh, T. Current states and future views in photodynamic therapy. *J.*  
37  
38  
39 *Photochem. Photobiol., C.* **2011**, *12*, 46-67.

40  
41  
42 (12) Ethirajan, M.; Chen, Y.; Joshi, P.; Pandey, R. K. The role of porphyrin chemistry  
43  
44  
45 in tumor imaging and photodynamic therapy. *Chem. Soc. Rev.* **2011**, *40*, 340-362.

1  
2  
3  
4 (13) Staron, J.; Boron, B.; Karcz, D.; Szczygiel, M.; Fiedor, L. Recent progress in  
5  
6  
7 chemical modifications of chlorophylls and bacteriochlorophylls for the applications in  
8  
9  
10 photodynamic therapy. *Curr. Med. Chem.* **2015**, *22*, 3054-3074.

11  
12  
13  
14  
15 (14) Cheng, Y.; A, C. S.; Meyers, J. D.; Panagopoulos, I.; Fei, B.; Burda, C. Highly  
16  
17  
18 efficient drug delivery with gold nanoparticle vectors for in vivo photodynamic therapy of  
19  
20  
21 cancer. *J. Am. Chem. Soc.* **2008**, *130*, 10643-10647.

22  
23  
24  
25  
26 (15) Allison, R. R.; Downie, G. H.; Cuenca, R.; Hu, X.-H.; Childs, C. J.; Sibata, C. H.  
27  
28  
29 Photosensitizers in clinical PDT. *Photodiagnosis Photodyn. Ther.* **2004**, *1*, 27-42.

30  
31  
32  
33  
34 (16) Hongying, Y.; Fuyuan, W.; Zhiyi, Z. Photobleaching of chlorins in homogeneous  
35  
36  
37 and heterogeneous media. *Dyes Pigm.* **1999**, *43*, 109-117.

38  
39  
40  
41  
42 (17) Turksoy, A.; Yildiz, D.; Akkaya, E. U. Photosensitization and controlled  
43  
44  
45 photosensitization with BODIPY dyes. *Coord. Chem. Rev.* **2019**, *379*, 47-64.

1  
2  
3  
4 (18) Kue, C. S.; Ng, S. Y.; Voon, S. H.; Kamkaew, A.; Chung, L. Y.; Kiew, L. V.; Lee,  
5  
6  
7 H. B. Recent strategies to improve boron dipyrromethene (BODIPY) for photodynamic  
8  
9  
10 cancer therapy: an updated review. *Photochem. Photobio. Sci.* **2018**, *17*, 1691-1708.

11  
12  
13  
14 (19) Loudet, A.; Burgess, K. BODIPY dyes and their derivatives: syntheses and  
15  
16  
17 spectroscopic properties. *Chem. Rev.* **2007**, *107*, 4891-4932.

18  
19  
20  
21 (20) Kamkaew, A.; Lim, S. H.; Lee, H. B.; Kiew, L. V.; Chung, L. Y.; Burgess, K.  
22  
23  
24 BODIPY dyes in photodynamic therapy. *Chem. Soc. Rev.* **2013**, *42*, 77-88.

25  
26  
27 (21) Awuah, S. G.; You, Y. Boron dipyrromethene (BODIPY)-based photosensitizers  
28  
29  
30 for photodynamic therapy. *RSC Adv.* **2012**, *2*, 11169-11183.

31  
32  
33 (22) Ge, Y.; O'Shea, D. F. Azadipyrromethenes: from traditional dye chemistry to  
34  
35  
36 leading edge applications. *Chem. Soc. Rev.* **2016**, *45*, 3846-3864.

37  
38  
39 (23) Agazzi, M. L.; Ballatore, M. B.; Durantini, A. M.; Durantini, E. N.; Tomé, A. C.  
40  
41  
42 BODIPYs in antitumoral and antimicrobial photodynamic therapy: An integrating review.  
43  
44  
45  
46  
47  
48  
49  
50  
51  
52  
53 *J. Photochem. Photobiol., C* **2019**, *40*, 21-48.

1  
2  
3 (24) Durantini, A. M.; Greene, L. E.; Lincoln, R.; Martinez, S. R.; Cosa, G. Reactive  
4  
5  
6  
7 Oxygen Species Mediated Activation of a Dormant Singlet Oxygen Photosensitizer: From  
8  
9  
10 Autocatalytic Singlet Oxygen Amplification to Chemically Controlled Photodynamic Therapy. *J.*  
11  
12  
13  
14 *Am. Chem. Soc.* **2016**, *138*, 1215-1225.  
15  
16  
17

18 (25) Gayathri, T.; Vijayalakshmi, A.; Mangalath, S.; Joseph, J.; Rao, N. M.; Singh, S.  
19  
20  
21 P. Study on Liposomal Encapsulation of New Bodipy Sensitizers for Photodynamic  
22  
23  
24  
25 Therapy. *ACS Med. Chem. Lett.* **2018**, *9*, 323-327.  
26  
27  
28

29 (26) Loudet, A.; Burgess, K. BODIPY dyes and their derivatives: syntheses and  
30  
31  
32 spectroscopic properties. *Chem. Rev.* **2007**, *107*, 4891-4932.  
33  
34  
35  
36

37 (27) Zhang, J.; Wang, N.; Ji, X.; Tao, Y.; Wang, J.; Zhao, W. BODIPY-based fluorescent  
38  
39  
40 probes for biothiols. *Chem. – Eur. J.* **2020**, *26*, 4172-4192.  
41  
42  
43  
44

45 (28) Yogo, T.; Urano, Y.; Ishitsuka, Y.; Maniwa, F.; Nagano, T. Highly efficient and  
46  
47  
48 photostable photosensitizer based on BODIPY chromophore. *J. Am. Chem. Soc.* **2005**,  
49  
50  
51  
52 *127*, 12162-12163.  
53  
54  
55  
56  
57  
58  
59  
60

1  
2  
3  
4 (29) Yang, Y.; Guo, Q.; Chen, H.; Zhou, Z.; Guo, Z.; Shen, Z. Thienopyrrole-expanded  
5  
6  
7 BODIPY as a potential NIR photosensitizer for photodynamic therapy. *Chem. Commun.*  
8  
9  
10 **2013**, *49*, 3940-3942.

11  
12  
13  
14 (30) Xiong, H.; Zhou, K.; Yan, Y.; Miller, J. B.; Siegwart, D. J. Tumor-activated water-  
15  
16  
17 soluble photosensitizers for near-infrared photodynamic cancer therapy. *ACS Appl.*  
18  
19  
20  
21 *Mater. Interfaces* **2018**, *10*, 16335-16343.

22  
23  
24  
25 (31) Zou, J.; Yin, Z.; Wang, P.; Chen, D.; Shao, J.; Zhang, Q.; Sun, L.; Huang, W.;  
26  
27  
28  
29 Dong, X. Photosensitizer synergistic effects: D-A-D structured organic molecule with  
30  
31  
32 enhanced fluorescence and singlet oxygen quantum yield for photodynamic therapy.  
33  
34  
35  
36 *Chem. Sci.* **2018**, *9*, 2188-2194.

37  
38  
39  
40 (32) Lim, S. H.; Thivierge, C.; Nowak-Sliwinska, P.; Han, J.; van den Bergh, H.;  
41  
42  
43  
44 Wagnieres, G.; Burgess, K.; Lee, H. B. In vitro and in vivo photocytotoxicity of boron  
45  
46  
47 dipyrromethene derivatives for photodynamic therapy. *J. Med. Chem.* **2010**, *53*, 2865-  
48  
49  
50  
51 2874.

1  
2  
3  
4 (33) He, H.; Lo, P. C.; Yeung, S. L.; Fong, W. P.; Ng, D. K. Synthesis and in vitro  
5  
6  
7 photodynamic activities of pegylated distyryl boron dipyrromethene derivatives. *J. Med.*  
8  
9  
10 *Chem.* **2011**, *54*, 3097-3102.

11  
12  
13  
14 (34) Zhou, Y.; Cheung, Y. K.; Ma, C.; Zhao, S.; Gao, D.; Lo, P. C.; Fong, W. P.; Wong,  
15  
16  
17 K. S.; Ng, D. K. P. Endoplasmic reticulum-localized two-photon-absorbing boron  
18  
19  
20  
21  
22 dipyrromethenes as advanced photosensitizers for photodynamic therapy. *J. Med. Chem.*  
23  
24  
25 **2018**, *61*, 3952-3961.

26  
27  
28  
29 (35) Watley, R. L.; Awuah, S. G.; Bio, M.; Cantu, R.; Gobeze, H. B.; Nesterov, V. N.;  
30  
31  
32  
33 Das, S. K.; D'Souza, F.; You, Y. Dual functioning thieno-pyrrole fused BODIPY dyes for  
34  
35  
36  
37 NIR optical imaging and photodynamic therapy: singlet oxygen generation without heavy  
38  
39  
40 halogen atom assistance. *Chem. Asian J.* **2015**, *10*, 1335-1343.

41  
42  
43  
44 (36) Sun, W.; Zhao, X.; Fan, J.; Du, J.; Peng, X. Boron dipyrromethene nano-  
45  
46  
47  
48 photosensitizers for anticancer phototherapies. *Small* **2019**, *15*, 1804927.

1  
2  
3 (37) Killoran, J.; Allen, L.; Gallagher, J. F.; Gallagher, W. M.; O'Shea, D. F. Synthesis  
4  
5  
6  
7 of BF<sub>2</sub> chelates of tetraarylazadipyrromethenes and evidence for their photodynamic  
8  
9  
10 therapeutic behaviour. *Chem. Commun.* **2002**, 1862-1863.

11  
12  
13  
14 (38) Gorman, A.; Killoran, J.; O'Shea, C.; Kenna, T.; Gallagher, W. M.; O'Shea, D. F.  
15  
16  
17 In vitro demonstration of the heavy-atom effect for photodynamic therapy. *J. Am. Chem.*  
18  
19  
20  
21  
22 *Soc.* **2004**, *126*, 10619-10631.

23  
24  
25 (39) Gallagher, W.; Allen, L.; O'shea, C.; Kenna, T.; Hall, M.; Gorman, A.; Killoran, J.;  
26  
27  
28  
29 O'Shea, D. A potent nonporphyrin class of photodynamic therapeutic agent: cellular  
30  
31  
32  
33 localisation, cytotoxic potential and influence of hypoxia. *Br. J. Cancer* **2005**, *92*, 1702-  
34  
35  
36  
37 1710.

38  
39  
40 (40) Byrne, A.; O'connor, A.; Hall, M.; Murtagh, J.; O'Neill, K.; Curran, K.; Mongrain, K.;  
41  
42  
43  
44  
45  
46  
47  
48  
49  
50  
51  
52  
53  
54  
55  
56  
57  
58  
59  
60  
Rousseau, J.; Lecomte, R.; McGee, S. Vascular-targeted photodynamic therapy with BF<sub>2</sub>-  
chelated Tetraaryl-Azadipyrromethene agents: a multi-modality molecular imaging  
approach to therapeutic assessment. *Br. J. Cancer* **2009**, *101*, 1565-1573.

1  
2  
3  
4 (41) Frimannsson, D. O.; Grossi, M.; Murtagh, J.; Paradisi, F.; O'Shea, D. F. Light  
5  
6  
7 induced antimicrobial properties of a brominated boron difluoride (BF<sub>2</sub>) chelated  
8  
9  
10 tetraarylazadipyrromethene photosensitizer. *J. Med. Chem.* **2010**, *53*, 7337-7343.

11  
12  
13  
14  
15 (42) Zhang, Q.; Cai, Y.; Wang, X. J.; Xu, J. L.; Ye, Z.; Wang, S.; Seeberger, P. H.; Yin,  
16  
17  
18 J. Targeted photodynamic killing of breast cancer cells employing heptamannosylated  
19  
20  
21 beta-cyclodextrin-mediated nanoparticle formation of an adamantane-functionalized  
22  
23  
24  
25 BODIPY photosensitizer. *ACS Appl. Mater. Interfaces* **2016**, *8*, 33405-33411.

26  
27  
28  
29 (43) Liu, Y.; Song, N.; Li, Z.; Chen, L.; Xie, Z. Near-infrared nanoparticles based on  
30  
31  
32  
33 aza-BDP for photodynamic and photothermal therapy. *Dyes Pigm.* **2019**, *160*, 71-78.

34  
35  
36  
37 (44) Wang, Q.; Ng, D. K. P.; Lo, P.-C. Functional aza-boron dipyrromethenes for  
38  
39  
40  
41 subcellular imaging and organelle-specific photodynamic therapy. *J. Mater. Chem. B*  
42  
43  
44 **2018**, *6*, 3285-3296.

45  
46  
47  
48 (45) Adarsh, N.; Shanmugasundaram, M.; Avirah, R. R.; Ramaiah, D. Aza-BODIPY  
49  
50  
51  
52 derivatives: enhanced quantum yields of triplet excited states and the generation of  
53  
54  
55  
56  
57  
58  
59  
60

1  
2  
3  
4 singlet oxygen and their role as facile sustainable photooxygenation catalysts. *Chem. –*  
5  
6  
7 *Eur. J.* **2012**, *18*, 12655-12662.  
8

9  
10  
11 (46) Gawale, Y.; Adarsh, N.; Kalva, S. K.; Joseph, J.; Pramanik, M.; Ramaiah, D.;  
12  
13  
14 Sekar, N. Carbazole-linked near-infrared Aza-BODIPY dyes as triplet sensitizers and  
15  
16  
17 photoacoustic contrast agents for deep-tissue imaging. *Chem. – Eur. J.* **2017**, *23*, 6570-  
18  
19  
20  
21  
22 6578.  
23

24  
25  
26 (47) Xiao, W.; Wang, P.; Ou, C.; Huang, X.; Tang, Y.; Wu, M.; Si, W.; Shao, J.; Huang,  
27  
28  
29 W.; Dong, X. 2-Pyridone-functionalized Aza-BODIPY photosensitizer for imaging-guided  
30  
31  
32  
33 sustainable phototherapy. *Biomaterials* **2018**, *183*, 1-9.  
34

35  
36  
37 (48) Gut, A.; Lapok, L.; Drelinkiewicz, D.; Pedzinski, T.; Marciniak, B.; Nowakowska,  
38  
39  
40 M. Visible-light photoactive, highly efficient triplet sensitizers based on iodinated Aza-  
41  
42  
43 BODIPYs: synthesis, photophysics and redox properties. *Chem. Asian J.* **2018**, *13*, 55-  
44  
45  
46  
47  
48 65.  
49

50  
51  
52 (49) Adarsh, N.; Avirah, R. R.; Ramaiah, D. Tuning photosensitized singlet oxygen  
53  
54  
55 generation efficiency of novel aza-BODIPY dyes. *Org. Lett.* **2010**, *12*, 5720-5723.  
56  
57

1  
2  
3  
4 (50) Zhao, M.; Xu, Y.; Xie, M.; Zou, L.; Wang, Z.; Liu, S.; Zhao, Q. Halogenated Aza-  
5  
6  
7 BODIPY for imaging-guided synergistic photodynamic and photothermal tumor therapy.  
8  
9  
10 *Adv. Healthcare Mater.* **2018**, *7*, 1800606.

11  
12  
13  
14  
15 (51) Zhao, W.; Carreira, E. M. Conformationally restricted aza-BODIPY: highly  
16  
17  
18 fluorescent, stable near-infrared absorbing dyes. *Chem. – Eur. J.* **2006**, *12*, 7254-7263.  
19  
20

21  
22  
23 (52) Zhao, W.; Carreira, E. M. Conformationally restricted aza-bodipy: a highly  
24  
25  
26 fluorescent, stable, near-infrared-absorbing dye. *Angew. Chem. Int. Ed.* **2005**, *44*, 1677-  
27  
28  
29 1679.  
30  
31

32  
33  
34 (53) Niedre, M.; Patterson, M. S.; Wilson, B. C. Direct near-infrared luminescence  
35  
36  
37 detection of singlet oxygen generated by photodynamic therapy in cells in vitro and  
38  
39  
40 tissues in vivo. *Photochem. Photobiol.* **2002**, *75*, 382-391.  
41  
42

43  
44  
45 (54) Moan, J.; Berg, K. The photodegradation of porphyrins in cells can be used to  
46  
47  
48 estimate the lifetime of singlet oxygen. *Photochem. Photobiol.* **1991**, *53*, 549-553.  
49  
50  
51

1  
2  
3  
4 (55) Ogilby, P. R. Singlet oxygen: there is still something new under the sun, and it is  
5  
6  
7 better than ever. *Photochem. Photobiol. Sci.*, **2010**, *9*, 1543-1560.  
8  
9

10  
11 (56) Kulsı, G.; Song, J. Sub cellular organelles-targeting photo dynamic therapy (PDT).  
12  
13  
14 *Mini Rev. Org. Chem.* **2016**, *13*, 336-348.  
15  
16  
17

18  
19 (57) Lv, W.; Zhang, Z.; Zhang, K. Y.; Yang, H.; Liu, S.; Xu, A.; Guo, S.; Zhao, Q.; Huang,  
20  
21  
22 W. A mitochondria-targeted photosensitizer showing improved photodynamic therapy  
23  
24  
25 effects under hypoxia. *Angew. Chem. Int. Ed.* **2016**, *55*, 9947-9951.  
26  
27  
28

29  
30 (58) Wang, H.; Chang, J.; Shi, M.; Pan, W.; Li, N.; Tang, B. A dual-targeted organic  
31  
32  
33 photothermal agent for enhanced photothermal therapy. *Angew. Chem. Int. Ed.* **2019**, *58*,  
34  
35  
36  
37 1057-1061.  
38  
39

40  
41 (59) Li, M.; Long, S.; Kang, Y.; Guo, L.; Wang, J.; Fan, J.; Du, J.; Peng, X. De novo  
42  
43  
44 design of phototheranostic sensitizers based on structure-inherent targeting for enhanced  
45  
46  
47  
48 cancer ablation. *J. Am. Chem. Soc.* **2018**, *140*, 15820-15826.  
49  
50  
51

1  
2  
3 (60) Chakraborty, S.; Agrawalla, B. K.; Stumper, A.; Vegi, N. M.; Fischer, S.; Reichardt,  
4  
5  
6  
7 C.; Kogler, M.; Dietzek, B.; Feuring-Buske, M.; Buske, C.; Rau, S.; Weil, T. Mitochondria  
8  
9  
10 targeted protein-ruthenium photosensitizer for efficient photodynamic applications. *J. Am.*  
11  
12  
13  
14 *Chem. Soc.* **2017**, *139*, 2512-2519.  
15  
16  
17

18 (61) Kessel, D.; Oleinick, N. L. Cell death pathways associated with photodynamic  
19  
20  
21  
22 therapy: an update. *Photochem. Photobiol.* **2018**, *94*, 213-218.  
23  
24  
25

26 (62) Mroz, P.; Yaroslavsky, A.; Kharkwal, G. B.; Hamblin, M. R. Cell death pathways in  
27  
28  
29  
30 photodynamic therapy of cancer. *Cancers (Basel)* **2011**, *3*, 2516-2539.  
31  
32  
33

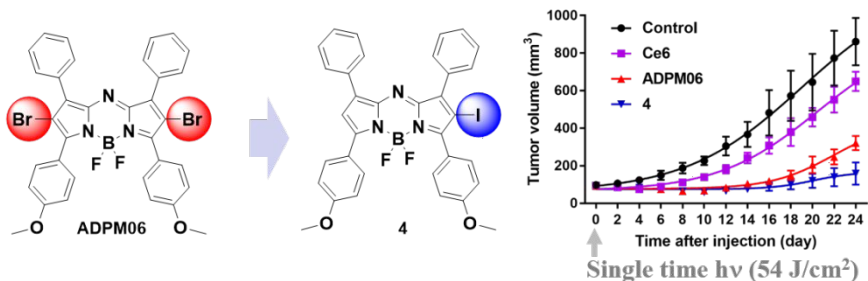
34 (63) Huang, L.; Li, Z.; Zhao, Y.; Zhang, Y.; Wu, S.; Zhao, J.; Han, G. Ultralow-power  
35  
36  
37  
38 near infrared lamp light operable targeted organic nanoparticle photodynamic therapy. *J.*  
39  
40  
41 *Am. Chem. Soc.* **2016**, *138*, 14586-14591.  
42  
43  
44

45 (64) Li, M.; Xiong, T.; Du, J.; Tian, R.; Xiao, M.; Guo, L.; Long, S.; Fan, J.; Sun, W.;  
46  
47  
48  
49 Shao, K.; Song, X.; Foley, J. W.; Peng, X. Superoxide radical photogenerator with  
50  
51  
52  
53  
54  
55  
56  
57  
58  
59  
60 amplification effect: surmounting the achilles' heels of photodynamic oncotherapy. *J. Am.*  
*Chem. Soc.* **2019**, *141*, 2695-2702.

(65) Fan, W.; Yung, B.; Huang, P.; Chen, X. Nanotechnology for multimodal synergistic cancer therapy. *Chem. Rev.* **2017**, *117*, 13566-13638.

(66) Maree, M. D.; Kuznetsova, N.; Nyokong, T. Silicon octaphenoxypthalocyanines: photostability and singlet oxygen quantum yields. *J. Photochem. Photobiol. A: Chem.* **2001**, *140*, 117-125.

### Table of Contents Graphic



**Intense NIR absorption / High photo-toxicity / Low dark-toxicity**  
**Good thermal-stability / High photo-stability / Excellent *in vivo* efficacy**